Title

Oligomerization Alters Binding Affinity between Amyloid Beta and a Modulator of Peptide Aggregation

Journal

The Journal of Physical Chemistry C, 121(43)

ISSN

1932-7447

Authors

Hilt, Silvia
Rojalin, Tatu
Viitala, Tapani
et al.

Publication Date

2017-11-02

DOI

10.1021/acs.jpcc.7b06164

Peer reviewed

HHS Public Access

Author manuscript

J Phys Chem C Nanomater Interfaces. Author manuscript; available in PMC 2018 November 02.

Published in final edited form as:

J Phys Chem C Nanomater Interfaces. 2017 November 2; 121(43): 23974–23987. doi:10.1021/acs.jpcc.7b06164.

Oligomerization Alters Binding Affinity Between Amyloid Beta and a Modulator of Peptide Aggregation

Silvia Hilt[1,‡], **Tatu Rojalin**[2,3,‡], **Tapani Viitala**[3], **Artturi Koivuniemi**[3], **Alex Bunker**[3], **Sebastian Wachsmann Hogiu**[2,4], **Tamás Kálai**[5], **Kálmán Hideg**[5], **Marjo Yliperttula**[3,6], and **John C. Voss**[1,*]

[1]Department of Biochemistry & Molecular Medicine, University of California, Davis, CA 95616, USA [2]Department of Pathology and Laboratory Medicine, and Center for Biophotonics, University of California Davis, USA [3]Centre for Drug Research, Division of Pharmaceutical Biosciences, University of Helsinki, Finland [4]Intellectual Ventures/Global Good, Bellevue, WA, USA [5]Institute of Organic and Medicinal Chemistry, University of Pécs, H 7624 Pécs, Szigeti st. 12. Pécs, Hungary [6]Department of Pharmaceutical Sciences, University of Padova, Italy

Abstract

The soluble oligomeric form of the amyloid beta (Aβ) peptide is the major causative agent in the molecular pathogenesis of Alzheimer's disease (AD). We have previously developed a pyrroline-nitroxyl fluorene compound (SLF) that blocks the toxicity of Aβ. Here we introduce the multi-parametric surface plasmon resonance (MP-SPR) approach to quantify SLF binding and effect on the self-association of the peptide via a label-free, real-time approach. Kinetic analysis of SLF binding to Aβ and measurements of layer thickness alterations inform on the mechanism underlying the ability of SLF to inhibit Aβ toxicity and its progression towards larger oligomeric assemblies. Depending on the oligomeric state of Aβ, distinct binding affinities for SLF are revealed. The Aβ monomer and dimer uniquely possess sub-nanomolar affinity for SLF via a non-specific mode of binding. SLF binding is weaker in oligomeric Aβ, which displays an affinity for SLF on the order of 100 μM. To complement these experiments we carried out molecular docking and molecular dynamics simulations to explore how SLF interacts with the Aβ peptide. The MP-SPR results together with *in silico* modeling provide affinity data for the SLF-Aβ interaction and allow us to develop a new general method for examining protein aggregation.

Graphical abstract

* jcvoss@ucdavis.edu.
‡S.H. and T.R. contributed equally to this work

Supporting Information

The following content is provided as Supporting Information:

- Additional experimental and theoretical considerations for MP-SPR.
- Expanded Table of affinity values determined for alternative Aβ configurations.
- Demonstration of native Aβ binding to tethered Aβ.
- Controls for non-specific binding to the sensor surface.
- Figure illustrating the Interaction kinetics fitting using the 1:1 fitting model
- Plot of inter-molecular contacts for simulations at elevated temperature.
- Further Description of Monomeric Aβ simulation with one or two SLF molecules.
- Animation of a longer simulation illustrating the dynamic Aβ-SLF interaction.

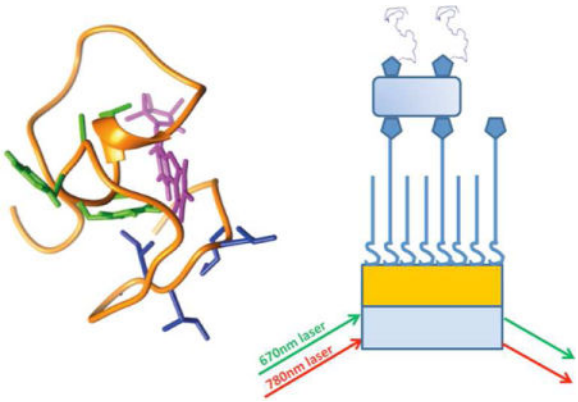

Introduction

Alzheimer's Disease (AD) is a progressive, devastating neurodegenerative disease that currently affects nearly five million people in the US alone. The incidence of AD is expected to triple by 2050[1]. Although the etiology of AD is complex, multiple lines of genetic, histological and biochemical evidence suggests the amyloid peptide (Aβ) is the primary causative agent[2]. The Aβ is constitutively released in the brain through proteolytic processing of the amyloid precursor protein (APP), which is, in turn, cleaved sequentially by β and γ secretases, two aspartyl proteases. Both the rate and site of APP cleavage, as well as the efficiency of Aβ clearance determine eventual neuropathology. Aβ is an intrinsically disordered peptide that undergoes a dynamic aggregation pattern that can ultimately lead to Aβ plaques deposited in the brain[3–4]

Importantly, numerous studies have established that the soluble oligomeric form of Aβ (AβO) represents the neurotoxic form of the peptide[5–7] Hence, there is significant interest in identifying compounds that inhibit Aβ oligomerization. To date, a diverse set of small molecules have been found to interfere with Aβ oligomerization and amyloid fibril formation, although the binding coordination and structural mechanism for inhibition remains unknown[8–12]. A major obstacle to the development of such therapeutic agents is the dynamic structure of the soluble Aβ peptide; toxicity results from various oligomeric forms present throughout the aggregation pathway[13].

We have previously shown that a novel, bifunctional compound can block both Aβ toxicity and oligomer growth[14–15]. This small molecule, named spin-labeled fluorene (SLF), contains a fluorene moiety for Aβ-targeting as well as a nitroxide spin label (Fig. 1). Biophysical studies indicate that SLF disrupts and inhibits oligomer growth[14–15]. The protective effect of SLF against Aβ toxicity is augmented by the free radical scavenging property of the nitroxide spin label[14, 16], which is efficient in addressing the strong oxidative element of AD pathogenesis[17–20].

Although the toxic state of Aβ is ill-defined, multiple lines of evidence correlate toxicity with oligomers on the order of 10-60 kDa that contain a high degree of conformational disorder distributed amongst oligomers in dynamic equilibrium (reviewed in[21]). Depending on the conditions, these oligomers progress to larger aggregates or transition into fibrillar-

competent species. Obtaining a quantitative description of Aβ structure and toxicity remains a challenge, and the dynamic nature of oligomeric Aβ further complicates efforts to address the mechanism of small molecule modulators of Aβ toxicity. We have therefore employed a label-free approach using surface-immobilized Aβ to measure SLF binding affinity to different oligomeric states of the peptide. The method, multi-parametric surface plasmon resonance (MP-SPR), is additionally useful because it also detects changes in layer thickness[22], and thereby provides information on how small molecule binding can modulate Aβ self-association.

MP-SPR is a powerful technique for studying label-free biomolecular interaction measured in real-time, providing detailed analysis of affinity and kinetics of small molecule interactions as well as a unique method for measuring peptide and protein self-assembly[23]. Here we use MP-SPR to investigate how spin labeled fluorenes decrease Aβ self-assembly and aggregation. The measurements provide kinetic constants for distinct SLF-Aβ interaction modes, leading to a better understanding of the role SLF plays in modulating Aβ aggregation and toxicity. Furthermore, by calculating layer thickness, the molecular masses deposited onto the MP-SPR sensors are modeled in terms of oligomer size. We demonstrate that MP-SPR is an effective tool for observing Aβ self-assembly and evaluating agents that can modulate peptide aggregation. Finally, we carried out molecular dynamics simulations of the SLF-Aβ interaction, providing insights into possible conformational states that correlate to a lowered toxicity and aggregation propensity for the Aβ peptide. This work represents a continuation in our development of the synergistic combination of label-free analytics and molecular dynamics to obtain key mechanistic insights of pharmaceutical relevance[24] The developed methodology represents a *biofunctional assay platform* where the biological environment is mimicked in order to enhance the *in vivo* relevance of the study. This platform can be extended to other similar systems where the modulation of disordered peptide aggregation is a potential therapeutic target.

Experimental Methods

Materials

Hexafluoro-2-propanol (HFIP) was purchased from Sigma-Aldrich (catalog number 105228-25G, St. Louis, MO). Dimethyl sulfoxide (DMSO) was purchased from Fisher Scientific (catalog number D12345, Pittsburgh, PA). Biotin-PEG-SH was purchased from Nanocs Inc. (catalog number PG2-BNTH-5k, New York, NY). 11-Mercapto-1-undecanol ($HS(CH_2)_{11}OH$) was obtained from Sigma Aldrich, St. Louis, MO (catalog number 447528-1G). The thiols were used as received. Streptavidin was purchased from Thermo Scientific (catalog number 43-4301, Pittsburgh, PA). Biotin was purchased from Sigma Aldrich (catalog number B4501-500MG) St. Louis, MO). β-amyloid peptide (1-40) (**Seq:** DAEFRHDSGYEVHHQKLVFFAEDV GS NKGAIIGLMVGGVV) and Biotin labeled β-amyloid peptide (1-40) (**Seq:** Biotin-DAEFRHDSGY EVHHQKLVFFAEDVGSNKGAIIGLMVGGVV) were purchased from EZBiolab Inc., Carmel, IN. Spin-labeled fluorene HO-4160 (SLF) was synthesized as described in[16].

Preparation of amyloid beta (Aβ) peptide samples

Aqueous preparations of predominately monomeric or oligomeric Aβ were made in solutions where conditions (pH, ionic strength, peptide concentration and incubation times) either increase or decrease the rate of oligomer formation[25–26]. The predominance of monomeric and oligomeric species was confirmed by dynamic light scattering (see below), consistent with previous measurements using fluorescence correlation spectroscopy[15]. To prepare monomers of biotinylated or native Aβ, the Aβ peptide was dissolved in HFIP and incubated at room temperature with gentle rocking for 48-72 hours. Vacuum evaporation was then used to remove the HFIP, resulting in a monomeric Aβ pellet. Immediately before the given experiment, the HFIP-treated pellet was warmed to room temperature and reconstituted in 10 μL of fresh DMSO. To produce monomeric peptide, the Aβ in DMSO stock solution was subsequently diluted in low ionic strength buffer (25 mM Tris, 1 mM EDTA, pH 8.0) to a 10 μM final concentration of the peptide monomer and the sample used immediately[27].

To obtain oligomeric Aβ (AβO), the DMSO Aβ stock was diluted into high ionic strength buffer (25 mM Tris, 150 mM NaCl, pH 7.0) to a final concentration of 40 μM and allowed to incubate at room temperature for 4 hours. Just prior to MP-SPR measurements the AβO solution was centrifuged at 15,000 × g for 5 minutes for amorphous aggregate removal. The supernatant contained the AβO used for MP-SPR measurements. As demonstrated previously[14, 27] these oligomeric preparations are anti-amyloid (A11)-positive oligomers, with a 40 μM solution producing particles at 4-hours of ~10 nm in diameter by AFM imaging. The AβO 40 μM solutions were diluted to 10 μM in high aggregation buffer just prior to injection into MP-SPR fluidic channels.

To produce SLF labeled AβO, we treated the 4 hrs AβO incubations with either 80 μM SLF (1:2 Aβ/SLF molar ratio to saturate Aβ binding sites) or vehicle, and allowed these solutions to incubate at room temperature for 4 hrs. Just prior to MP-SPR measurements the AβO/SLF and AβO/vehicle solutions were centrifuged at 15,000 × g for 5 minutes, and the supernatant removed for MP-SPR measurements.

Characterization of monomer and oligomer preparations by dynamic light scattering

Particle size analysis of the Aβ monomer and oligomer solutions was carried out at using dynamic light scattering (DLS) with a Brookhaven 90Plus instrument that monitors scattered light at 90° to the excitation. For monomer samples, Aβ(1-40) was HFIP-treated and dried. Immediately before measurement, dried pellets were dissolved in DMSO and diluted into either low salt buffer, pH 8.0 (for monomeric preparations) or diluted into high salt buffer, pH 7.0 (for oligomeric preparations). Monomeric samples were measured for 20 minutes, immediately after solvation into aqueous buffer to a concentration of 10 μM. Oligomeric samples were first incubated for 4-hr incubation in high ionic strength buffer. All samples were filtered through 0.22 μm filter to remove dust particles and large amorphous aggregates just prior to measurement. The average hydrodynamic radius was calculated using the ZetaPlus Particle Sizing Software Version 3.57 (Brookhaven Instruments). The calculated hydrodynamic diameters of Aβ monomers was ~1.4 nm, while the AβO species have an average hydrodynamic radius of ~75 nm.

MP-SPR measurements

MP-SPR measurements were performed by using an SPR-Navi 200™ instrument (BioNavis Ltd., Tampere, Finland). The MP-SPR instrument allows for expanded SPR sensing, having the capability to record the full SPR angular spectra over a wide angular range (~ 40-78 degrees). The instrument was equipped with two different wavelength lasers (670 nm and 785 nm) for plasmon excitation in two independent fluidic channels, which are integral parts of a PDMS flow cell (volume of each flow cell 1 μL). The liquid flows were controlled via a peristaltic pump and a 12-port chromatography injector, the typical flow rates varying between 10-100 μL/min, and in this particular study, between 10-20 μL/min. The scanning angle feature and utilization of two or more wavelengths enables recording full SPR angular spectra (intensity of reflected light as a function of angle of incidence) in real time. These, in turn, can be used to model and calculate e.g. the layer thicknesses (d) and refractive indices (n) for the studied molecular layers as well as kinetic parameters for the interaction phenomena using well-established physical models. Additional technical details are given in Supporting Information.

Preparation of the gold sensors for MP-SPR measurements

We used the SPR Navi™ gold sensor slides SPR102-AU-10 (Au as the plasmonic layer, d = 50 nm) provided by BioNavis for all of our MP-SPR measurements. To functionalize the gold sensor surface we followed the standard protocol, as described by[23] and adapted it to using biotinylated Aβ peptide as the ligand layer as shown in Fig. 2. We constructed a supramolecular assembly composed of a self-assembled monolayer (SAM) to which we attached the biotinylated Aβ peptide to form the functionalized gold sensors. Before surface assembly, the plain gold sensors were cleaned with absolute ethanol, and dried with nitrogen gas. First, we reconstituted the 11-Mercapto-1-undecanol and the biotin-PEG-SH in absolute ethanol to form a MuOH: Biotin-PEG-thiol (85:15 mol %, 5mM) (MBP-thiol) SAM solution. An adsorbed biotinylated, self-assembled monolayer (SAM) was generated directly on the gold sensor; the mixed, MBP/PEG thiols have been shown to make a better self-assembly layer than PEG-thiol alone by resisting non-specific protein adsorption[23]. The gold sensors were then immediately immersed in an MBP-thiol SAM solution, in a glass Petri dish, gold face up, and incubated for at least 16hrs, at room temperature, in the dark and the MBP-thiol was allowed to adsorb onto the gold sensor. The Petri dish was sealed with wax paper to prevent evaporation. Subsequently, the gold sensors were removed from the solution, washed in absolute ethanol and dried with nitrogen gas and loaded into the instrument. The second molecular layer was constructed by immobilization of streptavidin monitored *in situ* with the MP-SPR instrument, as 200 μg/ml of Streptavidin in DI water, was flowed over the MBP-thiol SAM sensor surface at 10 μl/min. After a stable baseline was obtained we proceeded to build the third molecular layer by injecting 10μM biotinylated Aβ in low aggregation buffer (25 mM Tris, 1 mM EDTA, pH 8.0) at 10μL/min, followed by low aggregation buffer until a stable baseline was noted. For the control channel we followed the same procedure for the first and second layer, except that the third layer was built by injecting 300 μL of 1mM biotin, at 10 μl/min until a stable baseline was noted. Binding of native Aβ to the tethered biotinylated Aβ was detected by measuring the shift in the SPR peak minimum (θ_{SPR}) before and after each sample injection. Example data are provided in Fig. S1.

To investigate SLF/Aβ binding, various SLF dilutions (10 μM, 20 μM, 30 μM, 40 μM) in low ionic strength buffer, pH 8.0, were flowed over the biotinylated Aβ biosensor surface at the concentrations indicated in the figures. Non-specific binding to the MBP-thiol SAM layer was tested by application of the same SLF dilutions over the MBP-Thiol SAM/ Streptavidin/biotin surface without Aβ. Similarly, to check for non-specific binding of Aβ to the MBP-thiol SAM layer, 10 μM of non-biotinylated (native) Aβ was flowed over the MBP-Thiol SAM/Streptavidin/biotin surface (See Fig. S2), followed by layer thickness analysis.

Physical principles of the interaction kinetics analysis

Kinetic analyses were performed using the SPR Navi™ Data Viewer 4.0 (BioNavis Ltd., Tampere, Finland) and the TraceDrawer 1.6 software (Ridgeview Instruments AB, Vänge, Sweden) - data shown in Table 1. Graphs in all figures were constructed using OriginPro 8.6 (Northampton, Massachusetts, USA). We started the kinetic analysis by selecting the desired interactions of each particular scheme. The kinetic fitting is based on the sensorgrams, which show the change in the SPR resonance angle (i.e. change in the SPR peak minimum (θ_{SPR})) as a function of time. We performed the analysis of SLF interactions in 4 different schemes; (i) SLF interacting with biotinylated Aβ, (ii) with native (non-biotinylated) Aβ, (iii) with AβO, and (iv) with AβO pretreated with SLF at a molar ratio of 1:2. The sensorgrams were baseline corrected by using a baseline level correction algorithm. Consequently, the bulk- and baseline-corrected sensorgrams were processed in the fitting phase with two different binding models within the TraceDrawer 1.6 software. SLF-Aβ interaction schemes were best fit using the 1:2 model appropriate for binding to two independent targets on a solid support. The mathematical description of the two used models is extensively described elsewhere (e.g.[28–29]). As the refractive properties of DMSO can change the bulk conditions quite drastically, the fitting was performed by taking into account the possible bulk effect the DMSO may have had during the experiment. The injection of an analyte dissolved in the DMSO typically induces a clear shift in the total internal reflection (TIR) angle. Since the full SPR angular spectrum is recorded, the bulk correction can be performed by subtracting the contribution of the TIR shift from the overall change in the angular position of the SPR peak minimum.

Basic SPR theory and physical principles of experimental layer thickness modeling

The fundamental mathematical depiction of SPR is derived from the Maxwell's equations, and has been described profoundly for example in[29–32]. Briefly, when the matching of incident light photons and plasmons occurs, the resonance condition is met:

$$\frac{\omega}{c}\sqrt{\varepsilon_0}\sin\theta_0 = \frac{\omega}{c}\left(\frac{\varepsilon_1\varepsilon_2}{\varepsilon_1+\varepsilon_2}\right)^{\frac{1}{2}} \quad (1)$$

where c is the speed of light in vacuum, ω is the light frequency, θ_0 is the angle of incidence of the light beam, and ε_0, ε_1, ε_2 are the dielectric constants of the prism, the metal, and the medium in contact with it, respectively. In general, the dielectric constant ε and refractive

index n for a given material can be expressed in their complex forms as $\hat{n} = n + ik = \sqrt{\mu\hat{\varepsilon}}$, and $\hat{\varepsilon} = \varepsilon + i\varepsilon'$, where $\hat{n}$, n and k are the complex refractive index, real- and imaginary part of the complex refractive index, respectively. The quantity μ denotes permeability, occurring in Maxwell's equations. Since the majority of materials are non-magnetic at optical frequencies, μ can be approximated very close to 1. Similarly, $\hat{\varepsilon}$, ε and ε' are the complex dielectric constant, real- and imaginary part of the complex refractive index. As a sum of the definitions made here, the refractive index and dielectric constant are related as $\hat{n} = \sqrt{\hat{\varepsilon}}$.

For the layer thickness and refractive index calculations, the shape and quantities associated with the SPR spectra were utilized. The spectra can be described with Fresnel's equations as the reflectivity of a multilayered system for *p-polarized* light. In practice, the modeling and solving for the matrix formalism was performed by mathematical fitting tools, or dedicated software. The layer thicknesses and refractive indices of the thin bio-molecular layers were solved by the two-wavelength method with angular scanning in all our experiments[33–35]. LayerSolver 1.0.2 (BioNavis Ltd., Tampere, Finland) software was used for modeling and solving for the layer properties.

The thicknesses of the modeled layers were linked as common variables in the modeling performed with the LayerSolver, i.e. the layer thickness was expected to be the same for both wavelengths since the MP-SPR angular spectra were measured from the same spot in the upper and lower sample channels. The complex refractive index was input as an independent variable for background (pure metal layer) modeling, or as a linearly dependent variable between the two used wavelengths.

Molecular docking, molecular dynamics simulations and analysis

Autodock Vina 1.1.2[36] was utilized to find the most probable binding sites and free-energies for SLF at the surface of the Aβ peptide. We chose to carry out the initial docking calculations to the solution structure of Aβ (1-40) solved with NMR[37] The PDB code for the structure is 1IYT. The PDB structure consists of several different conformations for Aβ, but we chose to use only the first one since our aim was also to carry out 20 ns MD simulation (referred to as S1) for the peptide in water surroundings. The docking calculations were repeated for structures that were derived from S1 simulation (2 ns intervals). All nonpolar hydrogens of Aβ and SLF were merged to the corresponding heavy atoms, a prerequisite for Autodock docking calculations. In general, the docking parameters were kept to their default values. One rotatable dihedral present in the SLF molecules were set to flexible. The size of the docking grid was set to 47 Å × 47 Å × 47 Å, which overlaid the entire Aβ peptide.

All molecular dynamics simulations were carried out using the GROMACS 5.0.4 package[38] and the GROMOS54A7 force field[39]. The GROMOS54A7 force field parameters for SLF were generated with Automated Topology Builder (ATB) server version 2.2[40–41]. The SPC model was used for water molecules[42]. To maintain zero net charge in the simulated systems three Na^+ counter ions were added. All MD simulations were carried out under the isobaric–isothermal (NPT) ensemble with periodic boundary conditions. A time step of 2 fs was used for integrating the equations of motion. The v-rescale and Berendsen algorithms were

employed to maintain physiological temperature (except where indicated) at 310 K (0.1 ps $^{-1}$) and an isotropic pressure of 1 bar (1.0 ps^{-1})[43]. The cutoff for Lennard-Jones interactions were set to 1.4 nm. For long-range electrostatics the particle mesh Ewald (PME) method was employed with a real-space cutoff of 1.4 nm[44] The LINCS algorithm was applied to constrain all bonds[45]. The simulated systems consisted of one Aβ peptide, one SLF molecule (except one simulation where the SLF molecules were not present), three Na^+ counter ions and 4719 water molecules. Three different MD-simulations were carried out. The simulated system 1 (S1) consisted of only the Aβ peptide, ions and water molecules. This simulation was performed up to 20 ns as previously described, solely to obtain four independent initial docking conformations. In the simulation systems 2 (S2) and 3 (S3) the SLF molecule was initially present in the docking sites 1 and 2 that were produced by the initial docking calculation. S2 and S3 systems were simulated up to 100 ns. The secondary structure of the Aβ peptide was analyzed using the gmx do_dssp analysis tool included in the GROMACS simulation package[46]. The root mean square deviation (RMSD) of the Aβ peptide was analyzed with the gmx rms program. The number of contacts was calculated using the gmx mindist program, which is also included in the GROMACS simulation package. The maximum distance for contacts between SLF and Aβ atoms were set to 0.6 nm. VMD were used to visualize the docking and simulation results[47]

Results

General Considerations

We have shown in previous work that, the SLF small molecule binds to soluble Aβ oligomers and protects against Aβ-induced cell death[14–15]. To characterize the binding of spin labeled fluorenes to Aβ, we employed real-time, label-free detection of SLF binding to biotinylated Aβ tethered to a self-assembled monolayer (SAM) as shown schematically in Fig. 2. The gold sensor surface is coated with biotin-functionalized (for streptavidin binding) PEG derivative [MuOH: Biotin-PEG-thiol (85:15 mol %)(MBP-Thiol SAM)]. The MBP-Thiol SAM surface is then coated with streptavidin, which immobilizes with high affinity and specificity to biotin. Injection of biotinylated Aβ results in the attachment of Aβ to the sensor surface through biotin binding to the available sites of the immobilized streptavidin. The analytes (SLF and/or Aβ) are then passed over the surface of immobilized Aβ, and SLF binding and/or Aβ self-association result in a change in the SPR signal response. The volume of all injections is 300 μL and flow rate is 10 μL/min for a total of 30 min injection time followed by 10 min of wash time for streptavidin, biotin, and Aβ, and 20 μL/min for SLF (20 min total injection time).

To determine if there is non-specific binding of Aβ and SLF to the layer surface, we used SPR signal changes from the baseline as an indicator of either SLF or non-biotinylated Aβ retained to the surface layer[48]. The absence of resonance signal increase above the baseline following injection washout demonstrates minimal non-specific interactions between the non-biotinylated Aβ peptide and SLF molecule with the MBP-Thiol SAM surface coated with streptavidin that do not significantly affect the binding kinetics calculations (see Fig. S2). We probed the Aβ and SLF interaction with the bare sensor chip surface by injecting the same concentrations of native (non-biotinylated) Aβ and SLF over the bare chip (Au)

surface and found no retention of either the Aβ or the SLF to the Au chip surface (data not shown).

Two separate wavelengths, 670 nm and 785 nm were used to record the signal responses in all MP-SPR measurements. However for reader simplification, only the 670 nm laser signals are shown in the sensorgrams and MP-SPR angular spectra. The mobile phase in the experiments consisted of the buffer specific to the form of Aβ applied in the MP-SPR analysis. The physicochemical characterization of SLF was performed in scenarios whereby different Aβ peptide compositions were mimicked and investigated. As described in Methods, predominantly monomeric Aβ was prepared at low ionic strength, slightly alkaline buffer and used immediately, whereas the sample of predominantly small oligomeric Aβ (AβO) was prepared in a neutral buffer containing 150 mM NaCl. Dynamic light scattering (DLS) measurements were performed to confirm that the low- and high-ionic strength conditions promote monomeric and oligomeric peptide, respectively. As determined by the DLS, monomeric Aβ in low ionic strength buffer displays a mean diameter of 1.4 nm, in agreement with earlier measurements of the Aβ monomer[26]. In contrast, the 4-hour AβO species in high ionic strength buffer have an average hydrodynamic radius of 75 nm.

SLF binds Aβ monomer with a very high affinity

We first measured the SLF binding kinetics to the immobilized monomeric Aβ alone. Affinity measurements were carried out by flowing increasing concentrations of SLF over the surface, which has been shown advantageous in the SPR study of high-affinity molecular interactions[49–51]. Serial injections of increasing concentrations of SLF over the biotinylated Aβ (Fig. 3) result in an increase in baseline maintained after the dissociation phase, indicative of SLF binding Aβ and retained as an Aβ/SLF complex.

Kinetics of SLF binding were best fitted according to a 1:2 binding model (Fig. 4), with a comparatively low χ^2 value = 34.39. The success of the fitting can also be estimated in the curves of Fig. 4, where the bold red line is the measured data, and the dotted line represents the fitting. This implies that the Aβ monomer can accommodate two molecules of SLF. With the 1:1 binding model, a substantially higher error (i.e. higher χ^2 values) is observed in the fit (Fig. S3, panels A and B). The 1:2 binding model generates two affinity constants, K_{D1} and K_{D2} (Table 1). Other parameters of the interaction kinetics analysis (k_{a1}, k_{d1}, etc.) are shown in Table S1 of Supporting Information. The first value, K_{D1} (~ 1.5×10^{-5} M) reflects a relatively strong binding of SLF (Table 1). However, the value for K_{D2} reveals an even stronger binding of SLF to Aβ, indicating binding at some sites is effectively irreversible on the time scale of these measurements. Because the calculation for K_{D2} carries a high level of uncertainty as determined within the time domain of these experiments, its value cannot be accurately determined. However, we can conclude that K_{D2} corresponds to a binding affinity of 1 nM or less. The lack of SLF dissociation is also reflected in the time-resolved presentation of the MP-SPR signals where the baseline raises after each concentration. The rates of SLF binding are also informative, consistent with a 2-step “induced fit” binding mechanism[52]. The value for k_{a2} (Table S1) in the order of 10^1 for SLF binding tethered Aβ indicates a relatively slow association rate. The value for k_{d2} is significantly smaller for the

same scenario, specific for a considerably slower dissociation rate. These differences are consistent with a slow on/off kinetic model for the binding of SLF to tethered Aβ.

SLF binds to non-biotinylated Aβ similar to biotinylated Aβ

To compare the binding of SLF to non-biotinylated (native) Aβ we injected 10 μM non-biotinylated Aβ over the biotinylated Aβ, at 10 μL/min for 30min, in low aggregation buffer. The low aggregation buffer prevents higher order oligomerization of Aβ, so we expect that some small scale dimerization to occur given the known affinity of Aβ for self-aggregation. Under these conditions, we predict a native monomer binding to the tethered Aβ, resulting in a *mostly dimeric species* on the surface. As shown in Fig. 5A, injection of the native monomer followed by buffer wash shows an increase from the baseline in the SPR signal. This increase is consistent with the native Aβ monomer pairing with the tethered Aβ species. The same effect is also reflected in layer thickness calculations showing that in the absence of SLF, ~34× more native Aβ associates with tethered Aβ forming a quasi-uniform layer of mostly dimeric Aβ (see below). After the baseline was stabilized, we injected the same series of increasing concentrations of SLF over the non-biotinylated (native) Aβ (Fig. 5A). The data indicate a similar binding pattern of SLF to both non-biotinylated and biotinylated Aβ. As with the tethered monomer alone, the data are best fitted by the 1:2 binding model (dashed line in Fig. 5B), consistent with monomeric and dimeric Aβ binding two molecules of SLF, with similar K_D values for each preparation (Table 1.). While k_{a2} and k_{d2} values for SLF/native Aβ interaction (Table S1) are indicative of the same slow on/off kinetic mechanism as for SLF/tethered Aβ, k_{a2} seems to be slower by an order of 10. As with tethered Aβ, native Aβ exhibits a second binding mode for SLF with significant lower affinity (k_{ai} and k_{d1}, Table S1). This result suggests that dimeric Aβ retains sub-nanomolar affinity for SLF as well as the capacity to bind SLF with two distinct affinities.

Oligomeric Aβ lacks very high binding affinity

We next investigated SLF binding to complexes of oligomeric Aβ (AβO) associated with the surface-immobilized Aβ. AβO was prepared in an aggregation-promoting buffer as described in *Experimental Procedures*, and measured by MP-SPR (Fig. 6, green trace). Kinetic analysis of the AβO/SLF complexes was initially performed using the 1:1 binding model that again yielded a substantially higher error (i.e. higher χ^2 values) than the 1:2 binding model. Thus, SLF binding to AβO is also best described by a model with two modes of ligand binding (Table 1; Fig. 7A). However, unlike the monomeric/dimeric preparations of Aβ, the $K_{D1\text{-}2}$ values of oligomeric samples are of the same order of magnitude (~10^{-4}-10^{-5} M), indicating that oligomer formation interferes with peptide adopting the high affinity conformation on the time-scale of these measurements. Thus, the pre-assembled AβO lacks the very high affinity binding, displaying a comparable lower affinity for SLF in both K_{D1} and K_{D2}. This finding suggests that monomeric/dimeric Aβ displays a uniquely high-affinity binding site for SLF, which may also serve to dock other amyloidophilic compounds as well.

In order to evaluate how SLF affects AβO binding, we compared the MP-SPR response of AβO applied over the surface of immobilized Aβ (Fig. 6, green trace) to AβO pre-incubated with a 2-fold molar ratio of SLF (Fig. 6, blue trace). As shown over the first two injections,

AβO without SLF pretreatment binds and sharply returns to the baseline value, however AβO with SLF pretreatment displays a prominent dissociation phase, suggesting that AβO pretreated with SLF is a more optically-active entity than AβO without SLF pretreatment. Thus the initial interaction signals induced by the pretreated AβO are also stronger. In addition, the dissociation of loosely bound SLF can be clearly seen for the case of pretreated AβO, as it resembles the dissociation kinetics observed when the compound is consecutively injected over AβO. As with the previous SLF binding schemes, the SLF binding to pretreated AβO was performed using the 1:2 binding model (Fig. 7B), which yields K_D values similar to AβO without SLF pretreatment (Table 1). Noteworthy are the injections of SLF after adsorption of AβO or AβO pretreated with SLF on the surface. As indicated by the smaller increase in the baseline of the sample pretreated with SLF (pretreated AβO; blue trace), a smaller net SLF binding is observed, consistent with this sample having a lower binding capacity for additional SLF.

SLF inhibits the self-association of Aβ

To investigate whether or not SLF inhibits the selfassociation of Aβ, we compared the binding of Aβ pre-mixed with SLF (at 1:2 molar ratio based on our previous two binding sites or modes results) with the binding of Aβ alone. Both sample solutions and flow solvent were in low aggregation conditions, favoring monomeric Aβ. As shown in Fig. 8, we flowed monomeric Aβ+SLF (blue trace) and monomeric Aβ alone (green trace) over the non-biotinylated Aβ immobilized on the sensor surface. The Aβ without SLF was retained on the sensor surface in a much higher amount, as revealed by the increase in the baseline (green trace) and Aβ+SLF was retained in a much lesser quantity as shown by the lower baseline (blue trace). This result is consistent with previous spectroscopic studies showing that SLF inhibits Aβ self-association[14–15].

SLF inhibition of Aβ oligomerization is detected by change in layer thickness

Since the theoretical findings[33–35], the multi-wavelength approach in MP-SPR for surface characterization has been successfully demonstrated in multiple applications[53–55]. The unique solution for the apparently interconnected thickness (d) and refractive index (n) of the sample layer can be found from the intersection of two continuum solutions, thus the MP-SPR measurements performed at multiple wavelengths can provide a direct indication of the layer thickness, thereby quantification of the mass added to the surface[53–54].

The MP-SPR angular spectra in Fig. 9 represent the experimental layer modeling procedure with intermediate steps shown, based on the data in Fig. 8. We started the modeling by determining first the background for our measured layer system, i.e. the metal (gold) layer. It should be noted that this background modeling step was performed with the inclusion of the SAM layer into the background calculation for two reasons; firstly, the contribution of SAM layer was considered very small to the measured MP-SPR angular spectra, and secondly, previous observations support the estimate that the calculation does not suffer from inaccuracies within the context of this analysis[55]. The layer after the streptavidin immobilization was measured next, and lastly the final situation after injection of the native Aβ monomer. A shift in the MP-SPR angular spectrum resonance angle to higher angles is observed as the peptide layer is building up in the lower sample channel (Fig. 9B and the

inset displaying the SPR peak minimum (θ_{SPR}) shift; see also Fig. 8A green trace). The corresponding shift is distinctly smaller in the MP-SPR angular spectrum representing the upper channel where the SLF was disrupting Aβ self-assembly and oligomerization (Fig. 9A and inset; see also Fig. 8A blue trace). The measured and modeled MP-SPR angular spectra at the end of the interactions are in relatively good agreement for both sample channel layers. Thus we can consider the calculated layer thicknesses (31.89 nm and 1.33 nm) and refractive indices (1.34070 and 1.37139, respectively) being relatively good and descriptive in the context of this analysis.

The layer thickness is clearly increased when SLF was not present in comparison to the situation where SLF was disrupting the self-assembly of the Aβ (Table 2). Furthermore, an interesting physical phenomenon can be observed in the refractive indices (RIs); the thinner layer (1.33 nm) without Aβ aggregation has a higher RI than the thicker layer (31.89 nm). This is in agreement with previous observations where a thin molecule layer can possess a higher RI than a thicker layer. Since the molecules can be assembled in a thin layer much more densely than in a sparse, aggregated layer, the light is also refracted more in a denser (but virtually thinner) layer. Another possibility lies in the different swelling properties of the layers; the water-based buffer content of the denser bio-molecule layer is smaller than the buffer content in the sparse, aggregated layer, thus resulting in the observed difference in refractive indices.

Molecular docking and molecular dynamics simulations as a computational tool for modeling SLF interaction with Aβ peptides

Molecular dynamic simulations were run to generate Aβ structures for exploring the most likely interaction sites for SLF at the surface of the Aβ peptide. First we carried out a single 20 ns long simulation of the Aβ monomer in water (referred to as S1; see Table 3), using an aqueous structure determined by NMR[37] as the initial Aβ conformation. To account for the inherent conformational disorder of the Aβ monomer in water, four intervals (5, 10, 15, 20 ns) from S1 were used for docking calculations and subsequent molecular dynamic simulations involving SLF. The RMSD results from S1 show the Aβ backbone is stabilized after 3 ns (Fig. 10A). In addition, the secondary structure of the Aβ peptide did not deviate considerably from the starting conformation (Fig. 10B), although minor changes as anticipated for its weakly ordered structure in solution[56–59]. We chose four structural snapshots starting from time points separated by 5 ns intervals for docking. The docking results for each interval are provided in Fig. 10C, showing the SLF docking geometry resulting in the lowest free energy of binding. For each unique starting Aβ conformation, comparably stable docking of SLF to Aβ is achieved. However, SLF does not dock to Aβ in a preferred manner despite achieving comparable binding energies (ranging from −7.5 to −6.8 kcal/mol) with each of the four starting conformations for the peptide. Rather the results indicate SLF interacts non-specifically with hydrophobic core I of Aβ (residues 17-21; green side chains in Fig. 10C), one of two hydrophobic cores (the other being residues 30-35; blue side chains in Fig. 10C) that are targets for agents blocking peptide assembly and toxicity[60–61]. These calculated binding energies are in good agreement with the SPR-derived binding free energies of −6.7 and −6.1 kcal/mol (K_{D1} with native biotinylated or non-biotinylated Aβ, respectively). Notably, these binding energies are on par

with those obtained by previously published simulations of Aβ and a bromofluorene containing a dimethyl-amino group in the position of our spin-label[60]. We therefore have a reasonable thermodynamic basis for the low docking free energies that are observed experimentally, consistent with an interaction between the Aβ peptide and SLF that does not involve a specific binding site. The consequences of the docked SLF on Aβ structure were subsequently examined with molecular dynamic simulation of the binary complex (see below).

Since the results of the docking calculations indicated that the interaction between the SLF with the Aβ peptide were strong yet mostly non-specific, we carried out two 100 ns long molecular dynamics simulations to follow the dynamics of the SLF molecule interacting with the Aβ peptide. These simulations were initiated from the lowest free-energy docking configurations of the 15 and 20 ns snapshots of S1 (Fig. 10), and are referred to as simulations S2 and S3, respectively. The snapshots and atomic contacts between the SLF molecules and the Aβ peptide revealed that the SLF molecule remains largely solvent exposed, but stays bound to the Aβ peptide during the entire simulation time in both S2 and S3 systems (Fig. 11).

By careful inspection of the simulation trajectories and atomic contacts it was found that the Aβ peptide can at least transiently fold around the SLF molecule during both simulations (See Fig. 11). To estimate the effect of a SLF induced binding pocket to its binding free-energy, we calculated the free energy of binding for S2 and S3 after 100 and 84 ns of simulation, respectively (see snapshots in Fig. 11). In these time points the Aβ peptide is folded around the SLF molecule to shield it better from aqueous surroundings. The docking calculation results showed that the refolding of Aβ around the SLF molecule increases the free energy of binding to −8.7 and −8.9 kcal/mol for S2 and S3, respectively. Because the structure and oligomerization kinetics of Aβ is highly sensitive to temperature[25], simulations from the S2 and S3 states were run at both 313 K and 350 K. Similar to the above simulations run at 310 K, the results reveal the SLF - Aβ complex is stable up to 200 ns at both of these higher temperatures (Fig. S4). The ability of SLF to remain largely shielded from solvent within the Aβ hairpin formed in either S2 or S3 up to at least 350 K is shown in **Animation 1**, Supporting Information. *[web enhanced object]*

Because MP-SPR indicates SLF binding with two distinct affinities, we also simulated the interaction of Aβ with two SLF molecules (see S4 in Table 3). Initially the two SLF molecules were randomly placed into the surrounding water phase, such that the SLF molecules were not in contact with the Aβ peptide at the beginning of the simulation. During the 150 ns simulation, both SLFs became bound to the surface of the Aβ peptide. After the number of contacts between the two SLF molecules and Aβ were in equilibrium (50 ns), we analyzed the minimum distances between each SLF and the C_α-atoms of the Aβ backbone as a function of amino acid sequence (Fig. S5). Compared to the case of the single SLF (S3 simulation, see Fig. S5), the plot of distances reveals a greater involvement of the C-terminal residues in the 2-SLF binding, and a slightly lower level of interaction with residues located in hydrophobic core I (positions 17-21). In addition, the two SLF molecules interact orthogonally, which places one of the ligands at a closer proximity to the central hairpin region (residues 23-26). Interestingly, if the SLF dimer is removed from the ternary

complex and a single SLF re-docked to form a binary SLF-Aβ complex, the binding energy of the remaining SLF rises to approximately −10.5 kcal/mol. This higher binding energy is closer to the energy expected for sub-nanomolar binding (on the order of −12 kcal/mol), suggesting a transient binding of SLF dimers may facilitate the formation of a higher affinity bindings state. While these simulations demonstrate energies sufficient to maintain peptide binding to both one and two SLF molecules, as well as clues to the residues involved, longer simulations are needed to fully elucidate the specific interactions between SLFs and Aβ peptides.

Discussion

As there is ample evidence in the literature that the neuronal damage in AD is derived from the toxicity of soluble Aβ oligomers[6, 62], there remains, however, much to be discovered regarding the toxicity of the Aβ oligomers due to the many faces of the complex aggregation pattern of Aβ. The relationship between function and structure is altered to a higher degree when a dynamic oligomerization/aggregation pattern yields oligomers with a large number of interchangeable, yet distinct conformational polymorphisms[63]. It is thus very possible that Aβ toxicity is associated with the process of aggregation and its many resulting species rather than a specific oligomeric state[21, 63–64].

These studies were carried out on $A\beta_{(1\text{-}40)}$, although $A\beta_{(1\text{-}42)}$ is recognized as the more neurotoxic species. We selected the $A\beta_{(1\text{-}40)}$ species to measure the interactions of a small molecule, SLF, because control over its aggregation state is much more manageable than it is for the longer peptide. Importantly, the 1-40 species shares the core regions known to interact with agents affecting amyloid formation and neurotoxicity[12, 61, 65–68]. In addition, the lower neurotoxicity of $A\beta_{(1\text{-}40)}$ does not necessarily diminish its relevance as a drug target. First, regarding the pool of soluble Aβ, $A\beta_{(1\text{-}40)}$ is typically 10× higher than $A\beta_{(1\text{-}42)}$, with $A\beta_{(1\text{-}40)}$ largely responsible for the closely associated Cerebral amyloid angiopathy (CAA) pathology. Second, oligomers *in vivo* are heterogeneous for both $A\beta_{(1\text{-}40)}$ and $A\beta_{(1\text{-}42)}$, and determining the influence of either peptide form with respect to the multiple cellular targets of Aβ is a long way from being understood.

The SLF interaction kinetics analysis was initiated using a relatively simple 1:1 interaction kinetics model. However, none of the experimental data in the four calculated scenarios satisfactorily fit to this model (χ^2 values being in the order of 500-700). Thus a 1:2 binding model was employed yielding a significantly more accurate fit to the data. In addition, the molecular docking simulations (discussed below) indicate a similar accommodation of 2 SLF molecules within a disordered Aβ monomer, further supporting the rationale for using the 1:2 binding model in the interaction kinetics calculations. For monomeric Aβ, K_{D1} of 15 μM and K_{D2} in the sub-nanomolar range were calculated. When SLF interacts with a surface comprised of native monomeric Aβ bound to a tethered Aβ monomer, K_{D1} (41 μM) and K_{D2} (sub-nanomolar) are on par with the tethered monomer. It is noteworthy that the lack of appreciable SLF dissociation within the high-affinity (K_{D2}) binding mode produces a relatively large degree of uncertainty in its calculated value. Although the current methodology cannot precisely generate K_{D2} values for the monomer/dimer samples, we have designated these affinities as “subnanomolar”, which represents a conservative upper

limit for the observed binding behavior. Nevertheless, these results indicate Aβ maintains a highly avid SLF binding in both the monomer or dimer states. A strong binding capability for SLF is also consistent with previous bioactivity measurements in cultured neurons, where SLF protects against Aβ toxicity in the nanomolar range[14]. For oligomeric Aβ, the affinity of AβO for SLF is substantially lower, with both K_{D1} and K_{D2} in the 100 μM range.

A caveat to these studies is our limitations in examining peptide that is homogenous for either monomer or defined oligomer. However, any method designed to capture a specific sate of Aβ is disrupting a dynamic equilibrium of self-associating, intrinsically disordered peptides that likely have distinguishable toxicity and cellular targets. In fact the complexity of Aβ aggregation and conformation partially explains the complexity of Alzheimer's pathogenesis[21]. Another caveat relates to whether the surface chemistry employed here affects the aggregation behavior of the peptide. Ryu et al reported non-specific binding of $Aβ_{(1-42)}$ to the MuOH SAM layer may affect the oligomerization state of Aβ, which was prevented by adding a dextran layer[69]. However their approach involved amine coupling chemistry, whereas we choose to use a biotin/streptavidin platform that offers very specific and strong binding for the biotinylated $Aβ_{(1-40)}$. Furthermore, we saturated the MuOH-biotin layer with streptavidin in an effort to offer the least amount of surface available for non-specific interaction between Aβ and surface layer, and similar to the role of Dextran in the above noted study, the PEG moiety in our configuration acts as an antifouling-agent to prevent unsolicited Aβ aggregation during the MP-SPR measurements. Given that we do not detect a fast aggregation component or layer thickness complication upon injection of the monomeric preparation, the influence of our surface chemistry on Aβ aggregation is minimal at best.

The simulations demonstrate a dynamic interaction of either one, two or three SLF molecules. Interestingly the 1:1 simulations (S2 and S3) show that SLF molecules preferentially reside closer to the two hydrophobic regions (amino acids 17-21 and 30-40) of Aβ that are presumed to interact with small hydrophobic molecules[60–61, 67, 70–71]. This suggests that the Aβ peptide is folded around the SLF molecule in a horseshoe-like fashion in which the close contact between backbone atoms of these hydrophobic regions is prohibited. It is interesting to note that this kind of interaction with SLF could hinder the formation of β-sheet structure of the Aβ peptides, thought to be a prerequisite for the formation of more stable amyloid fibrils[72]. Modeling also shows that the wrapping of the Aβ peptide around the ligands is also possible for a stoichiometry of 1:2, with a stack of two SLF molecules forming a dynamic interaction with the Aβ peptide. Thus, even though the interaction of SLF with the Aβ monomer is largely non-specific, simulations suggest SLF binding may induce interactions among residues leading to a more stable hairpin structure that sheilds the hydrophobic SLF ligand from water. We propose that the highest affinity state involves interactions with both of the peptide's two hydrophobic core regions. As readily apparent in **Animation 1**, this induced conformational change in Aβ creates in a hydrophobic pocket that can largely shield the SLF from the aqueous surroundings. Such a conformational change is consistent with the anti-oligomerization activity of SLF[14–15], since it would diminish the driving force of aggregation via the hydrophobic effect. Furthermore we have shown that SLF binding not only effects Aβ oligomerization, but also the backbone

structure of the peptide[15]. Taken together, an induced fit manner of SLF binding is consistent with the relatively slow on kinetics as measured by MP-SPR, whereas the induced compaction of Aβ structure around SLF following its binding may account for the very SLF off-rate observed in the monomer[52].

How then to consider the lower binding affinity that is also measured in the monomeric Aβ preparation? Since the monomeric condidtions inhibit, but do not abolish oligomer formation, the presence of residual AβO provides the most likely source of SLF binding with the lower K_{D1} affinity. Two facts support this contention: (i) K_{D1} is on the order of the the binding affinites measured for the AβO preparation, and (ii) MP-SPR measurements of native Aβ monomer binding to the preparation of tethered monomer Aβ demonstrates that self association of the peptide indeed occurs under the low aggregation conditions. Thus, since the hydrophobic residues also mediate interactions within unstructured oligomers, where the peptide is present in a disordered antiparallel arrangement[72–74], we surmise that inter-peptide interactions may preclude the high affinity binding conformation that is available to the monomer. In the oligomer, both K_D values are in the 100 micromolar range. It is likely that both binding modes involve a non-specific surface interaction of SLF with the peptide, and that the different affinities reflect the heterogeneous structures within the oligomers themselves.

Although SLF inhibits oligomer growth and reduces the size of preassembled oligomers, our previous fluorescence correlation spectroscopy (FCS) analyses indicate that these complexes assemble into a smaller, more stable form of AβO[15]. Thus, regardless of the mode of high affinity SLF binding in the monomer, initial thermodynamic forces driving monomeric Aβ and SLF interaction are not available in the oligomer. In addition to the steric factors discussed above, other considerations can be a reduction of the hydrophobic effect on binding once the peptide-SLF is buried in the oligomer or, given that SLF has both H-bond acceptors and donors, the interference of coordinating H-bonds by groups involved in intermolecular H-bonds. As discussed below, the consequences of SLF binding to Aβ are most profound with regard to oligomer growth. It is important to note that SLF does not exclude peptide-peptide interactions. The binding of SLF to dimers of Aβ is similar to that of monomeric Aβ. These findings are consistent with earlier FCS measurements[15] showing SLF-treated oligomers collapse and decrease significantly in size, but not completely to the monomeric state.

Layer thickness analysis provided additional support for the ability of SLF to slow the progression of Aβ oligomerization, by showing that there is significantly more Aβ deposited on the sensor surface in the absence of SLF than in the presence of SLF, in fact a factor of 30 more (Table 2). The optical modeling performed on the basis of the measured full SPR angular spectra yielded consistent results with the DLS measurements. In the presence of SLF and in low aggregation buffer conditions, the layer thickness is very close to the mean hydrodynamic diameter of Aβ measured by DLS in the low aggregation buffer (~1.4 nm). In the absence of SLF, and in the early stages of oligomerization, the optical modeling demonstrates that the thickness of the layer to be 31.9 nm. This is in accordance with DLS measurements (mean hydrodynamic diameter of ~ 75 nm for the AβO). By necessity, the conditions for the two different approaches are distinct, which may account for the smaller

apparent size of AβO observed by layer thickness. Nevertheless, the Aβ layer thickness grows towards the measured mean hydrodynamic diameter of AβO when SLF is not employed to prevent the oligomerization process. In addition, the results also underline the fact that the four different experimental schemes for investigating the physicochemical properties and interactions of SLF can be considered to have successfully addressed the progression of the monomeric, dimeric and oligomeric states of Aβ.

Based on docking calculations and MD simulations we suggest that the binding of SLF to the surface of Aβ is non-specific since the binding site and energies were seen to depend on the both the amino acid side chain conformations and secondary structure fluctuations. These results are verified by the experimental results that show binding energy is in rough agreement with our simulation results. Furthermore, the MD simulations indicated that the SLF remains at the surface of the Aβ peptide and can be surrounded or shielded by the peptide. The docking calculations produced binding free-energies on the order of −6 kcal/mol, comparable to the K_D-values produced by the experiments. Interestingly, when SLF was docked to the hairpin structure, the resulting binding free-energies (−8.7 and −8.9 kcal/mol) agreed very well with experimental values.

We were, however, not able to produce binding free-energies comparable with the highest K_D reported by the experiments. (~−12 kcal/mol). As seen in our simulations, it is possible that the structure of Aβ refolds when it interacts with SLF so that it can better shield the hydrophobic SLF molecule from its aqueous surroundings. Consequently, the shielding of SLF by the Aβ peptide could increase the binding free-energy of SLF considerably as was shown by our subsequent docking calculations. Admittedly, since Aβ is weakly structured, our simulations were clearly not able to sample the accessible phase space of this complex molecule completely, thus the specific highest K_D value conformations were probably missed for this reason. Our simulation results are in broad agreement with the majority of the experimental K_D measurements, however, indicating that the non-specific binding mechanism, involving alteration of the peptide to shield the SLF is a probable mechanism. A further, more rigorous simulation study, involving several simulations of microsecond lengths and greater, could find the higher K_D binding conformation; this research is currently being undertaken, however, it is beyond the scope of the current study. We hypothesize that the SLF molecule binds strongly to the surface of the Aβ peptide and modify its conformational fluctuations in a way that hinders the aggregation of the peptides. It is known that Aβ is mostly unfolded in the aqueous solution although it possesses transient structural fluctuations depending on the physicochemical surroundings[75–76]. Some of these transient structures such as β-sheets are more prone to the formation of initial peptide aggregation nuclei[77]; if the rate of occurrence of such structures is minimized by the presence of SLF or similar agents then this mechanism could be developed into a practical therapy for the inhibition of Aβ peptide aggregation and formation into neurotoxic amyloid fibrils.

Conclusions

In summary, in this work we have presented a novel hybrid experimental-computational analytical approach for elucidating the mechanisms for protein aggregation and small

molecules interactions relevant for the molecular pathogenesis of Alzheimer's disease. Experimental MP-SPR studies provided valuable kinetic binding data on a global macroscopic scale without the use of labeling agents, while molecular dynamics simulations provided a mechanistic view on the molecular scale. The new findings suggest that SLF not only prevents Aβ oligomerization, but that the effect is expected to be significantly greater in the early stage of peptide aggregation. In fact, this rationale for targeting monomeric Aβ prior to neurotoxic oligomer formation has been previously postulated[78]. To our knowledge, the findings present the first biomolecular layer thickness and refractive index evaluations to measure the accumulation and aggregation of Aβ, a process central to the elucidation of AD pathogenesis. The avidin-biotin interaction coupled with the PEG-SAM surface chemistry is suitable for aggregation prone, intrinsically disordered peptides, allowing for observation of selected stages of assembly. The MP-SPR approach, when coupled with screens for rapidly measuring Aβ toxicity[79], can provide a high-throughput identification of anti-amyloid candidates based on affinity, inhibition of peptide assembly, and bioactivity. Because other neurodegenerative diseases involve the aggregation of intrinsically disordered polypeptides, MP-SPR may circumvent experimental challenges of screening therapeutic candidates in those systems as well.

Supplementary Material

Refer to Web version on PubMed Central for supplementary material.

Acknowledgments

Financial support by the Academy of Finland (grants: #263861 and #292253), Tekes - the Finnish Funding Agency for Innovation EV-Extra-Tox project and the Professor Pool - Orion Research Foundation are gratefully acknowledged. CSC - The IT Center for Science (Helsinki, Finland) is acknowledged for providing supercomputer facilities. The authors also acknowledge support from the UC Davis STAIR Program to JCV. We thank Dr. David Gae for his assistance in rendering molecular structures.

References

1. Hebert LE, Weuve J, Scherr PA, Evans DA. Alzheimer Disease in the United States (2010-2050) Estimated Using the 2010 Census. Neurology. 2013; 80:1778–83. [PubMed: 23390181]
2. Viola KL, Klein WL. Amyloid Beta Oligomers in Alzheimer's Disease Pathogenesis, Treatment, and Diagnosis. Acta Neuropathol. 2015; 129:183–206. [PubMed: 25604547]
3. Walsh DM, Klyubin I, Fadeeva JV, Rowan MJ, Selkoe DJ. Amyloid-B Oligomers: Their Production, Toxicity and Therapeutic Inhibition. Biochem Soc Trans. 2002; 30:552–557. [PubMed: 12196135]
4. De Simone A, Kitchen C, Kwan AH, Sunde M, Dobson CM, Frenkel D. Intrinsic Disorder Modulates Protein Self-Assembly and Aggregation. Proc Natl Acad Sci U S A. 2012; 109:6951–6. [PubMed: 22509003]
5. Kayed R, Head E, Thompson JL, McIntire TM, Milton SC, Cotman CW, Glabe CG. Common Structure of Soluble Amyloid Oligomers Implies Common Mechanism of Pathogenesis. Science. 2003; 300:486–9. [PubMed: 12702875]
6. Klein WL, Stine WB Jr, Teplow DB. Small Assemblies of Unmodified Amyloid Beta-Protein Are the Proximate Neurotoxin in Alzheimer's Disease. Neurobiol Aging. 2004; 25:569–80. [PubMed: 15172732]
7. Cheon M, Chang I, Mohanty S, Luheshi LM, Dobson CM, Vendruscolo M, Favrin G. Structural Reorganisation and Potential Toxicity of Oligomeric Species Formed During the Assembly of Amyloid Fibrils. PLoS Comput Biol. 2007; 3:1727–38. [PubMed: 17941703]

8. Bartolini M, Bertucci C, Bolognesi ML, Cavalli A, Melchiorre C, Andrisano V. Insight into the Kinetic of Amyloid Beta (1-42) Peptide Self-Aggregation: Elucidation of Inhibitors' Mechanism of Action. ChemBioChem. 2007; 8:2152–61. [PubMed: 17939148]
9. Sgarbossa A. Natural Biomolecules and Protein Aggregation: Emerging Strategies against Amyloidogenesis. Int J Mol Sci. 2012; 13:17121–37. [PubMed: 23242152]
10. Aulic S, Bolognesi ML, Legname G. Small-Molecule Theranostic Probes: A Promising Future in Neurodegenerative Diseases. Int J Cell Biol. 2013; 2013:150952. [PubMed: 24324497]
11. Jameson LP, Smith NW, Dzyuba SV. Dye-Binding Assays for Evaluation of the Effects of Small Molecule Inhibitors on Amyloid (Abeta) Self-Assembly. ACS Chem Neurosci. 2012; 3:807–19. [PubMed: 23173064]
12. Wang Q, Yu X, Li L, Zheng J. Inhibition of Amyloid-Beta Aggregation in Alzheimer's Disease. Curr Pharm Des. 2014; 20:1223–43. [PubMed: 23713775]
13. Oddo S, Caccamo A, Smith IF, Green KN, LaFerla FM. A Dynamic Relationship between Intracellular and Extracellular Pools of Abeta. Am J Pathol. 2006; 168:184–94. [PubMed: 16400022]
14. Petrlova J, Kalai T, Maezawa I, Altman R, Harishchandra G, Hong HS, Bricarello DA, Parikh AN, Lorigan GA, Jin LW, et al. The Influence of Spin-Labeled Fluorene Compounds on the Assembly and Toxicity of the Abeta Peptide. PLoS One. 2012; 7:e35443. [PubMed: 22558151]
15. Altman R, Ly S, Hilt S, Petrlova J, Maezawa I, Kalai T, Hideg K, Jin LW, Laurence TA, Voss JC. Protective Spin-Labeled Fluorenes Maintain Amyloid Beta Peptide in Small Oligomers and Limit Transitions in Secondary Structure. Biochim Biophys Acta. 2015; 1854:1860–1870. [PubMed: 26374940]
16. Kalai T, Petrlova J, Balog M, Aung HH, Voss JC, Hideg K. Synthesis and Study of 2-Amino-7-Bromofluorenes Modified with Nitroxides and Their Precursors as Dual Anti-Amyloid and Antioxidant Active Compounds. Eur J Med Chem. 2011; 46:1348–55. [PubMed: 21333407]
17. Cai Z, Zhao B, Ratka A. Oxidative Stress and Beta-Amyloid Protein in Alzheimer's Disease. Neuromolecular Med. 2011; 13:223–50. [PubMed: 21901428]
18. Rosini M, Simoni E, Milelli A, Minarini A, Melchiorre C. Oxidative Stress in Alzheimer's Disease: Are We Connecting the Dots? J Med Chem. 2014; 57:2821–31. [PubMed: 24131448]
19. Sultana R, Butterfield DA. Role of Oxidative Stress in the Progression of Alzheimer's Disease. J Alzheimers Dis. 2010; 19:341–53. [PubMed: 20061649]
20. Rochet JC. Novel Therapeutic Strategies for the Treatment of Protein-Misfolding Diseases. Expert Rev Mol Med. 2007; 9:1–34.
21. Hubin E, van Nuland NA, Broersen K, Pauwels K. Transient Dynamics of Abeta Contribute to Toxicity in Alzheimer's Disease. Cell Mol Life Sci. 2014; 71:3507–21. [PubMed: 24803005]
22. Kubiak-Ossowska K, Cwieka M, Kaczynska A, Jachimska B, Mulheran PA. Lysozyme Adsorption at a Silica Surface Using Simulation and Experiment: Effects of Ph on Protein Layer Structure. Phys Chem Chem Phys. 2015; 17:24070–7. [PubMed: 26315945]
23. Ihalainen P, Majumdar H, Viitala T, Törngren B, Närjeoja T, Määttänen A, Sarfraz J, Härmä H, Yliperttula M, Österbacka R, et al. Application of Paper-Supported Printed Gold Electrodes for Impedimetric Immunosensor Development. Biosensors. 2013; 3:1–17. [PubMed: 25587396]
24. Bunker A, Magarkar A, Viitala T. Rational Design of Liposomal Drug Delivery Systems, a Review: Combined Experimental and Computational Studies of Lipid Membranes, Liposomes and Their Pegylation. Biochim Biophys Acta. 2016
25. Stine WB Jr, Dahlgren KN, Krafft GA, LaDu MJ. In Vitro Characterization of Conditions for Amyloid-Beta Peptide Oligomerization and Fibrillogenesis. J Biol Chem. 2003; 287:11612–22.
26. Snyder SW, Ladror US, Wade WS, Wang GT, Barrett LW, Matayoshi ED, Huffaker HJ, Krafft GA, Holzman TF. Amyloid-Beta Aggregation: Selective Inhibition of Aggregation in Mixtures of Amyloid with Different Chain Lengths. Biophys J. 1994; 67:1216–28. [PubMed: 7811936]
27. Hong HS, Maezawa I, Budamagunta M, Rana S, Shi A, Vassar R, Liu R, Lam KS, Cheng RH, Hua DH, et al. Candidate Anti-Abeta Fluorene Compounds Selected from Analogs of Amyloid Imaging Agents. Neurobiol Aging. 2010; 31:1690–1699. [PubMed: 19022536]

28. Karlsson R, Fält A. Experimental Design for Kinetic Analysis of Protein-Protein Interactions with Surface Plasmon Resonance Biosensors. J Immunol Methods. 1997; 200:121–133. [PubMed: 9005951]
29. Albers WM, Vikholm-Lundin I. Surface Plasmon Resonance on Nanoscale Organic Films. Springer; New York: 2011.
30. Maier SA. Plasmonics: Fundamentals and Applications. Springer Science & Business Media; 2007.
31. Hayt WH, Buck JA. Engineering Electromagnetics. 2001; 7
32. Sadowski JW, Korhonen IKJ, Peltonen JPK. Characterization of Thin Films and Their Structures in Surface Plasmon Resonance Measurements. OPTICAL ENGINEERING. 1995; 34:6.
33. Peterlinz K, Georgiadis R. Two-Color Approach for Determination of Thickness and Dielectric Constant of Thin Films Using Surface Plasmon Resonance Spectroscopy. Opt Commun. 1996; 130:260–266.
34. Zhou M, Otomo A, Yokoyama S, Mashiko S. Estimation of Organic Molecular Film Structures Using Surface-Plasmon Resonance Spectroscopy. Thin Solid Films. 2001; 393:114–118.
35. Grassi JH, Georgiadis RM. Temperature-Dependent Refractive Index Determination from Critical Angle Measurements: Implications for Quantitative Spr Sensing. Anal Chem. 1999; 71:4392–4396. [PubMed: 21662865]
36. Trott O, Olson AJ. Autodock Vina: Improving the Speed and Accuracy of Docking with a New Scoring Function, Efficient Optimization and Multithreading. J Computational Chemistry. 2010; 31:455–461.
37. Vivekanandan S, Brender JR, Lee SY, Ramamoorthy A. A Partially Folded Structure of Amyloid-Beta(1-40) in an Aqueous Environment. Biochem Biophys Res Commun. 2011; 411:312–316. [PubMed: 21726530]
38. Pronk S, Páll S, Schulz R, Larsson P, Bjelkmar P, Apostolov R, Shirts M, Smith J, Kasson P, van der Spoel D, et al. Gromacs 4.5: A High-Throughput and Highly Parallel Open Source Molecular Simulation Toolkit. Bioinformatics. 2013; 29:845–54. [PubMed: 23407358]
39. Schmid N, Eichenberger AP, Choutko A, Riniker S, Winger M, Mark AE, van Gunsteren WF. Definition and Testing of the Gromos Force-Field Versions 54a7 and 54b7. Eur Biophys J. 2011; 40:843–56. [PubMed: 21533652]
40. Malde AK, Zuo L, Breeze M, Stroet M, Poger D, Nair PC, Oostenbrink C, Mark AE. An Automated Force Field Topology Builder (Atb) and Repository: Version 1.0. J Chem Theory Comput. 2011; 7:4026–4037. [PubMed: 26598349]
41. Koziara K, Stroet M, Malde A, Mark A. Testing and Validation of the Automated Topology Builder (Atb) Version 2.0: Prediction of Hydration Free Enthalpies. J Comput Aided Mol Des. 2014; 28:221–233. [PubMed: 24477799]
42. Berendsen HJC, Postma JPM, van Gunsteren WF, Hermans J. Interaction Models for Water in Relation to Protein Hydration. In: Pullman B, editorIntermolecular Forces. D. Reidel Publishing Company; 1981. 331–342.
43. Berendsen HJC, Postma JPM, van Gunsteren WF, DiNola A, Haak JR. Molecular Dynamics with Coupling to an External Bath. J Chem Phys. 81:3684–3690.
44. Essmann U, Perera L, Berkowitz ML, Darden T, Lee H, Pedersen LG. A Smooth Particle Mesh Ewald Method. J Chem Phys. 1995; 103:8577–8593.
45. Hess B, Bekker H, Berendsen HJC, Fraaije JGEM. Lincs: A Linear Constraint Solver for Molecular Simulations. J Comput Chem. 1997; 18:18–1463.
46. Kabsch W, Sander C. Dictionary of Protein Secondary Structure: Pattern Recognition of Hydrogen-Bonded and Geometrical Features. Biopolymers. 1983; 22:2577–2637. [PubMed: 6667333]
47. Humphrey W, A D, Schulten K. Vmd: Visual Molecular Dynamics. J Mol Graph. 1996; 14:33–38. [PubMed: 8744570]
48. Sota H, Hasegawa Y, Iwakura M. Detection of Conformational Changes in an Immobilized Protein Using Surface Plasmon Resonance. Anal Chem. 1998; 70:2019–24. [PubMed: 9608841]
49. Karlsson R, Katsamba PS, Nordin H, Pol E, Myszka DG. Analyzing a Kinetic Titration Series Using Affinity Biosensors. Anal Biochem. 2006; 349:136–147. [PubMed: 16337141]

50. Myszka DG, Jonsen MD, Graves BJ. Equilibrium Analysis of High Affinity Interactions Using Biacore. Anal Biochem. 1998; 265:326–330. [PubMed: 9882410]
51. Palladino P, Aura A, Spoto G. Surface Plasmon Resonance for the Label-Free Detection of Alzheimer's ?-Amyloid Peptide Aggregation. Anal Bioanal Chem. 2015:1–6.
52. Gakamsky DM, Luescher IF, Pecht I. T Cell Receptor-Ligand Interactions: A Conformational Preequilibrium or an Induced Fit. Proc Natl Acad Sci U S A. 2004; 101:9063–6. [PubMed: 15178754]
53. Liang H, Miranto H, Granqvist N, Sadowski JW, Viitala T, Wang B, Yliperttula M. Surface Plasmon Resonance Instrument as a Refractometer for Liquids and Ultrathin Films. Sensors Actuators B: Chem. 2010; 149:212–220.
54. Granqvist N, Liang H, Laurila T, Sadowski J, Yliperttula M, Viitala T. Characterizing Ultrathin and Thick Organic Layers by Surface Plasmon Resonance Three-Wavelength and Waveguide Mode Analysis. Langmuir. 2013; 29:8561–8571. [PubMed: 23758623]
55. Granqvist N, Yliperttula M, Välimäki S, Pulkkinen P, Tenhu H, Viitala T. Control of the Morphology of Lipid Layers by Substrate Surface Chemistry. Langmuir. 2014; 30:2799–2809. [PubMed: 24564782]
56. Zhang S, Iwata K, Lachenmann MJ, Peng JW, Li S, Stimson ER, Lu Y, Felix AM, Maggio JE, Lee JP. The Alzheimer's Peptide a Beta Adopts a Collapsed Coil Structure in Water. J Struct Biol. 2000; 130:130–41. [PubMed: 10940221]
57. Lim KH, Henderson GL, Jha A, Louhivuori M. Structural, Dynamic Properties of Key Residues in Abeta Amyloidogenesis: Implications of an Important Role of Nanosecond Timescale Dynamics. ChemBioChem. 2007; 8:1251–4. [PubMed: 17549789]
58. Yan Y, Wang C. Abeta42 Is More Rigid Than Abeta40 at the C Terminus: Implications for Abeta Aggregation and Toxicity. J Mol Biol. 2006; 364:853–62. [PubMed: 17046788]
59. Yan Y, Liu J, McCallum SA, Yang D, Wang C. Methyl Dynamics of the Amyloid-Beta Peptides Abeta40 and Abeta42. Biochem Biophys Res Commun. 2007; 362:410–4. [PubMed: 17709094]
60. Li J, Liu R, Lam KS, Jin LW, Duan Y. Alzheimer's Disease Drug Candidates Stabilize a-Beta Protein Native Structure by Interacting with the Hydrophobic Core. Biophys J. 2011; 100:1076–82. [PubMed: 21320453]
61. Landau M, Sawaya MR, Faull KF, Laganowsky A, Jiang L, Sievers SA, Liu J, Barrio JR, Eisenberg D. Towards a Pharmacophore for Amyloid. PLoS Biol. 2011; 9:e1001080. [PubMed: 21695112]
62. Lesne S, Koh MT, Kotilinek L, Kayed R, Glabe CG, Yang A, Gallagher M, Ashe KH. A Specific Amyloid-Beta Protein Assembly in the Brain Impairs Memory. Nature. 2006; 440:352–7. [PubMed: 16541076]
63. Kayed R, Lasagna-Reeves CA. Molecular Mechanisms of Amyloid Oligomers Toxicity. J Alzheimers Dis. 2013; 33(Suppl 1):S67–78. [PubMed: 22531422]
64. Tiwari MK, Kepp KP. ?-Amyloid Pathogenesis: Chemical Properties Versus Cellular Levels. Alzheimer's & Dementia. 2016; 12:184–194.
65. Hard T, Lendel C. Inhibition of Amyloid Formation. J Mol Biol. 2012; 421:441–65. [PubMed: 22244855]
66. Dolphin GT, Ouberai M, Dumy P, Garcia J. Designed Amyloid Beta Peptide Fibril - a Tool for High-Throughput Screening of Fibril Inhibitors. ChemMedChem. 2007; 2:1613–23. [PubMed: 17876751]
67. Minicozzi V, Chiaraluce R, Consalvi V, Giordano C, Narcisi C, Punzi P, Rossi GC, Morante S. Computational and Experimental Studies on Beta-Sheet Breakers Targeting Abeta1-40 Fibrils. J Biol Chem. 2014; 289:11242–52. [PubMed: 24584938]
68. Nie Q, Du XG, Geng MY. Small Molecule Inhibitors of Amyloid Beta Peptide Aggregation as a Potential Therapeutic Strategy for Alzheimer's Disease. Acta Pharmacol Sin. 2011; 32:545–51. [PubMed: 21499284]
69. Ryu J, Joung H-A, Kim M-G, Park CB. Surface Plasmon Resonance Analysis of Alzheimer's B-Amyloid Aggregation on a Solid Surface: From Monomers to Fully-Grown Fibrils. Anal Chem. 2008; 80:2400–2407. [PubMed: 18303863]

70. Okuno H, Mori K, Okada T, Yokoyama Y, Suzuki H. Development of Aggregation Inhibitors for Amyloid-Beta Peptides and Their Evaluation by Quartz-Crystal Microbalance. Chem Biol Drug Des. 2007; 69:356–61. [PubMed: 17539828]

71. Hilbich C, Kisters-Woike B, Reed J, Masters CL, Beyreuther K. Substitutions of Hydrophobic Amino Acids Reduce the Amyloidogenicity of Alzheimer's Disease Beta A4 Peptides. J Mol Biol. 1992; 228:460–73. [PubMed: 1453457]

72. Ahmed M, Davis J, Aucoin D, Sato T, Ahuja S, Aimoto S, Elliott JI, Van Nostrand WE, Smith SO. Structural Conversion of Neurotoxic Amyloid-Beta(1-42) Oligomers to Fibrils. Nat Struct Mol Biol. 2010; 17:561–7. [PubMed: 20383142]

73. Cerf E, Sarroukh R, Tamamizu-Kato S, Breydo L, Derclaye S, Dufrene YF, Narayanaswami V, Goormaghtigh E, Ruysschaert JM, Raussens V. Antiparallel Beta-Sheet: A Signature Structure of the Oligomeric Amyloid Beta-Peptide. Biochem J. 2009; 421:415–23. [PubMed: 19435461]

74. Mitternacht S, Staneva I, Hard T, Irback A. Monte Carlo Study of the Formation and Conformational Properties of Dimers of Abeta42 Variants. J Mol Biol. 2011; 410:357–67. [PubMed: 21616081]

75. DuBay KF, Pawar AP, Chiti F, Zurdo J, Dobson CM, Vendruscolo M. Prediction of the Absolute Aggregation Rates of Amyloidogenic Polypeptide Chains. J Mol Biol. 2004; 341:1317–26. [PubMed: 15302561]

76. Chiti F, Stefani M, Taddei N, Ramponi G, Dobson CM. Rationalization of the Effects of Mutations on Peptide and Protein Aggregation Rates. Nature. 2003; 424:805–8. [PubMed: 12917692]

77. Fernandez-Escamilla AM, Rousseau F, Schymkowitz J, Serrano L. Prediction of Sequence-Dependent and Mutational Effects on the Aggregation of Peptides and Proteins. Nat Biotechnol. 2004; 22:1302–6. [PubMed: 15361882]

78. Cohen SI, Linse S, Luheshi LM, Hellstrand E, White DA, Rajah L, Otzen DE, Vendruscolo M, Dobson CM, Knowles TP. Proliferation of Amyloid-Beta42 Aggregates Occurs through a Secondary Nucleation Mechanism. Proc Natl Acad Sci U S A. 2013; 110:9758–63. [PubMed: 23703910]

79. Varghese K, Molnar P, Das M, Bhargava N, Lambert S, Kindy MS, Hickman JJ. A New Target for Amyloid Beta Toxicity Validated by Standard and High-Throughput Electrophysiology. PLoS One. 2010; 5:e8643. [PubMed: 20062810]

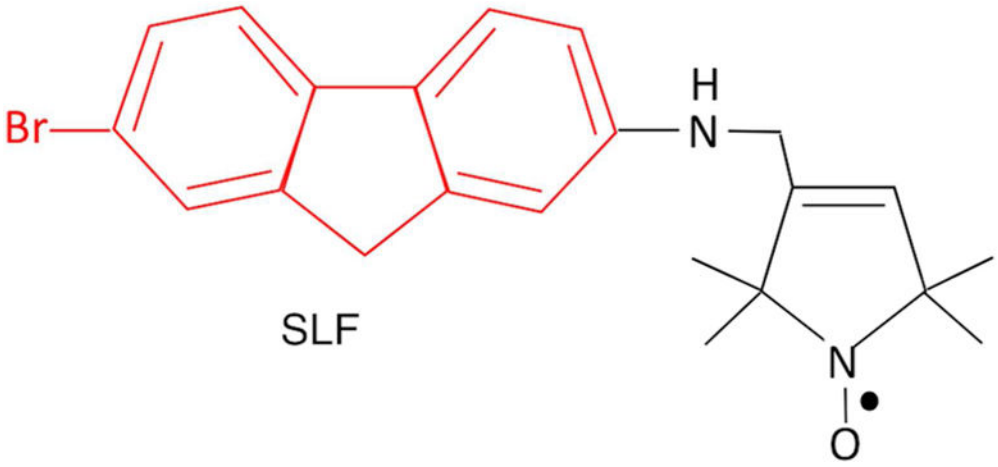

Fig. 1.

The chemical structure of spin-labeled fluorene (SLF), a novel compound that disrupts the formation of amyloid plaques. The amyloid binding moiety is shown in red, and the nitroxide spin label in black.

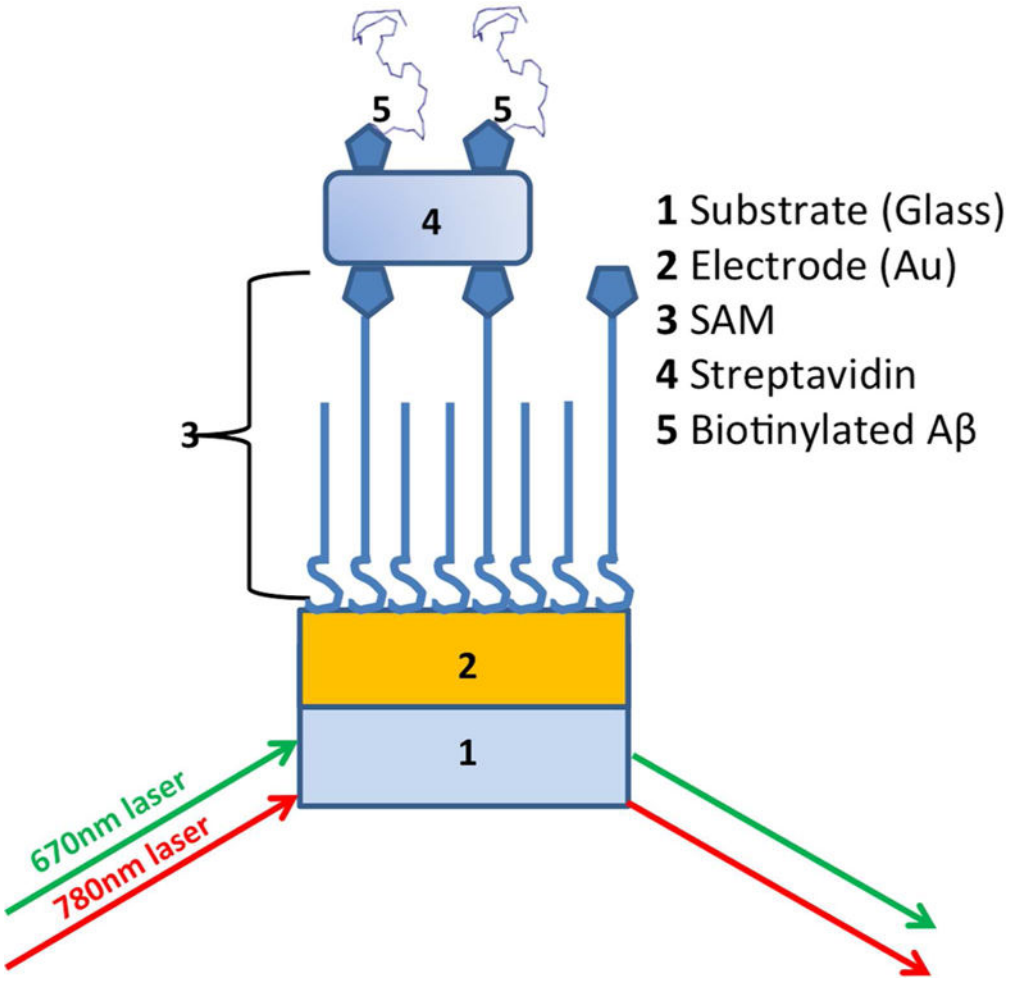

Fig. 2.

Schematic diagram of the MP-SPR sensor surface construction (the MBP-Thiol SAM/ streptavidin + biotinylated Aβ/analyte assembly). Details regarding the preparation of the gold sensors are provided in Experimental Procedures.

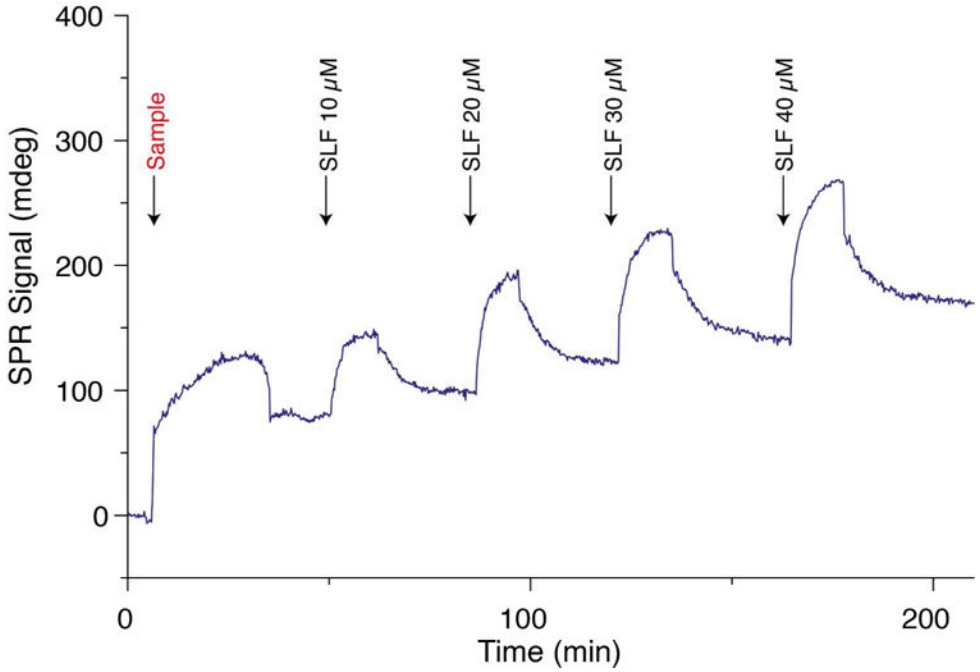

Fig. 3.

SLF binds biotinylated, monomeric Aβ with high affinity. MP-SPR signal response after injections of increasing concentrations of SLF (10, 20, 30, and 40 μM). The sensor surface was pre-coated with 10 μM biotinylated monomeric Aβ.

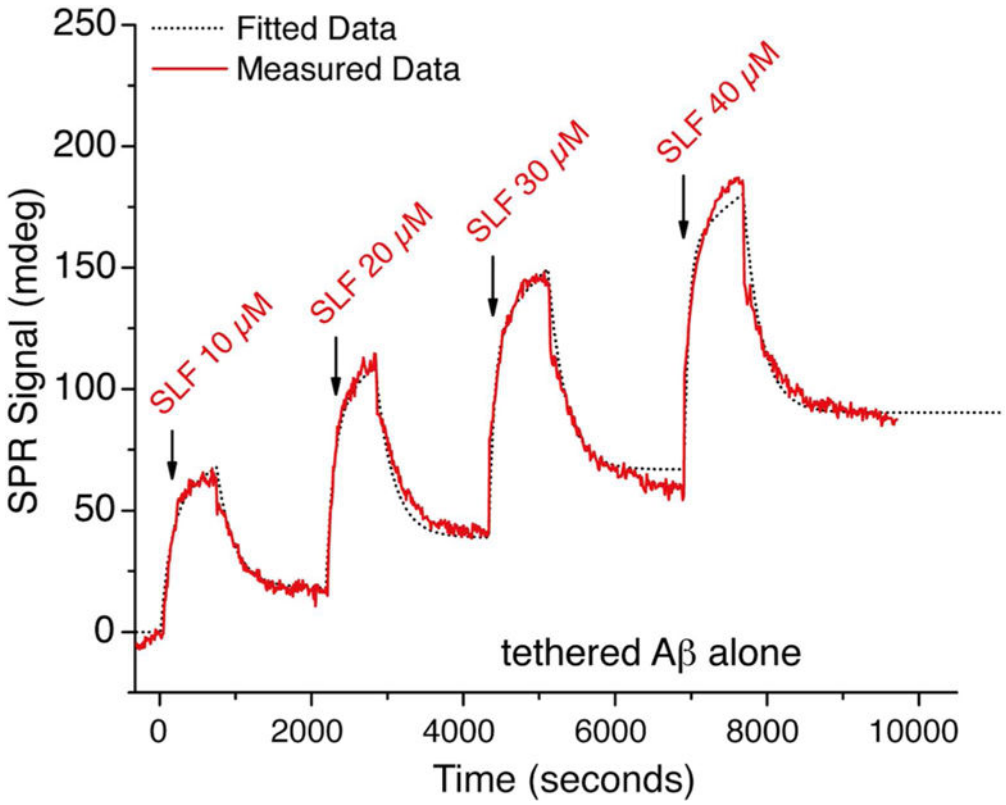

Fig. 4.

Binding kinetics show Aβ presents two binding sites. The sensorgrams are extracted from binding of SLF to the tethered monomers of biotinylated Aβ. The native Aβ monomer was injected at 10 μL/min, and the flow rate for SLF addition was 20 μL/min. The sensorgrams are shown as a red line, and the fits according to the 1:2 binding model are shown as a black dashed line. The kinetic parameters obtained from the fits are shown in Table 1.

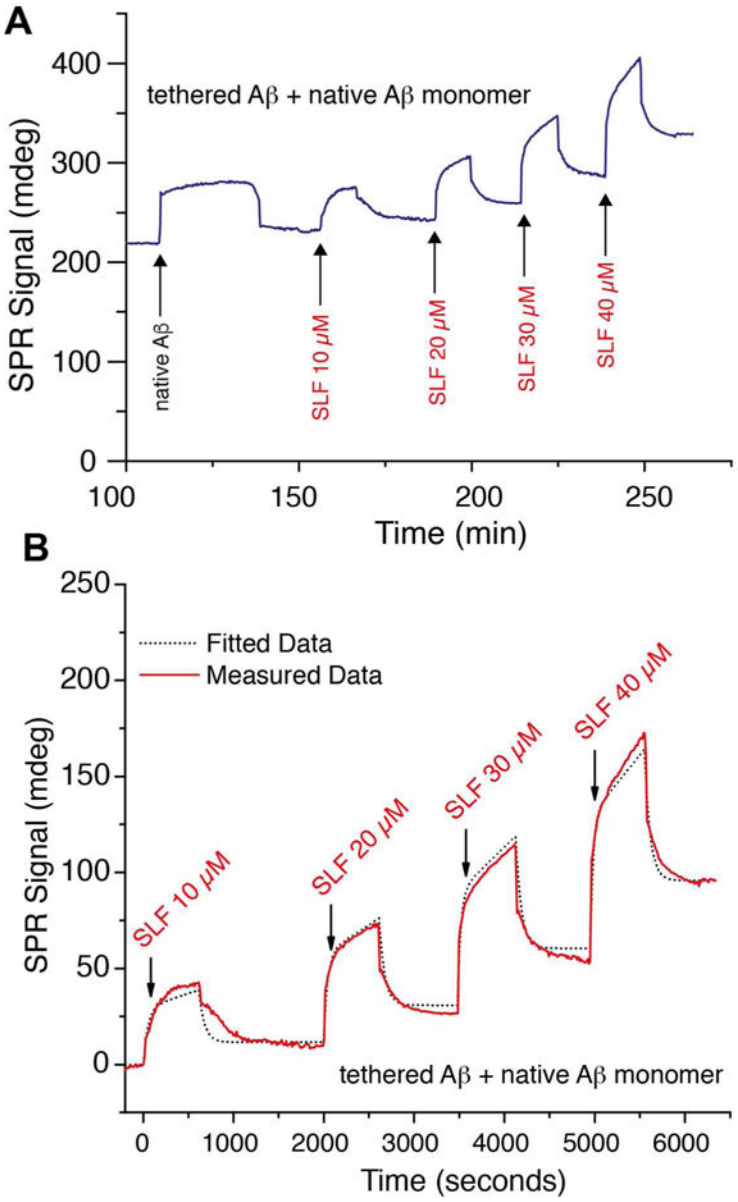

Fig. 5.

High affinity SLF binding is also observed with native monomeric Aβ. **A**. The MP-SPR signal response after injections of various concentrations of SLF, 10, 20, 30, and 40 μM to a sensor surface containing biotin-tethered Aβ monomer were coated with 10 μM native monomeric Aβ. SLF was injected at 20 μL/min. **B**. Binding kinetics of data in (A) fit (black dashed line) according to the 1:2 binding model. The kinetic parameters obtained from the fits are shown in Table 1.

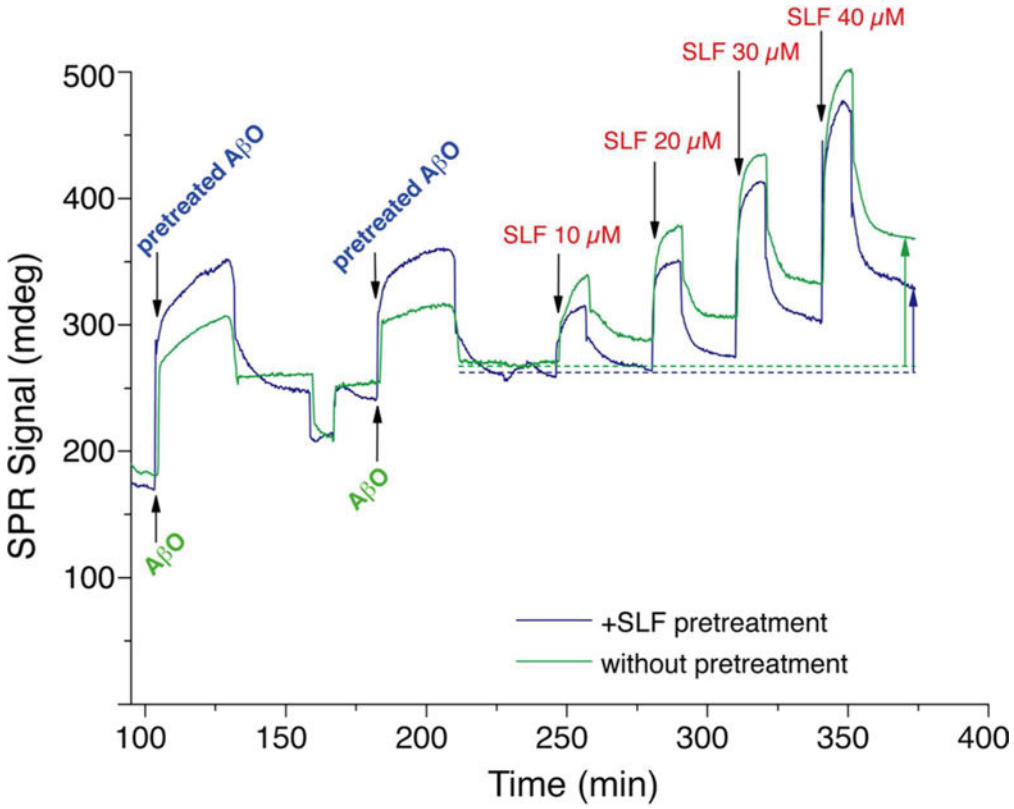

Fig. 6.

SLF binding to oligomeric Aβ (AβO). MP-SPR signal response after two successive injections of 10 μM AβO, with (blue trace) or without (green trace) pretreatment of the AβO with 20 μM SLF. After baseline stabilized, increasing concentrations (10, 20, 30 and 40 μM) of SLF were applied through both flow channels. Mobile phase consisted of the high ionic strength, pH 7.0 buffer.

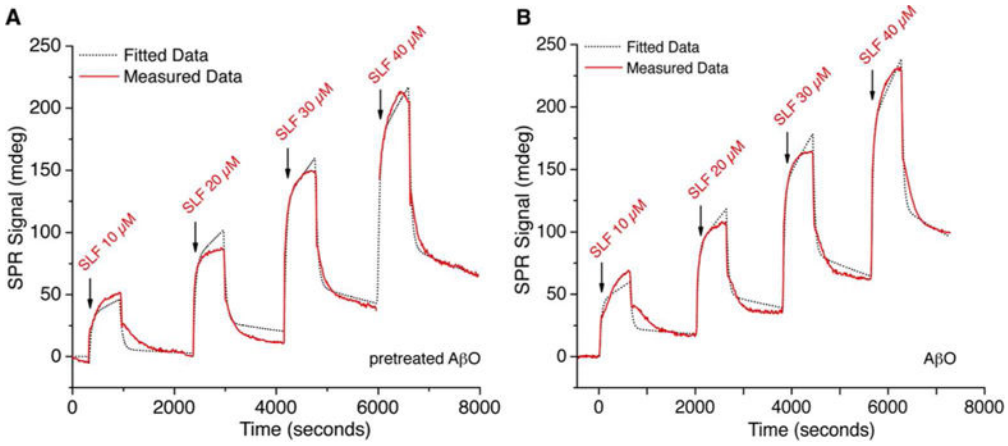

Fig.7.

Binding kinetics of SLF onto oligomeric Aβ. The sensorgrams are extracted from SLF binding to AβO associated with tethered monomers of biotinylated Aβ. The binding of SLF to AβO pretreated with 20 μM SLF is shown in Panel (**A**). The binding of SLF to AβO alone is shown in Panel (**B**). The AβO samples were injected at 10 μL/min, and the SLF solution's flow rate was 20 μL/min. The sensorgrams are shown as a red line, and the fits are shown as a black dashed line. The kinetic parameters obtained from the fits are shown in Table 1.

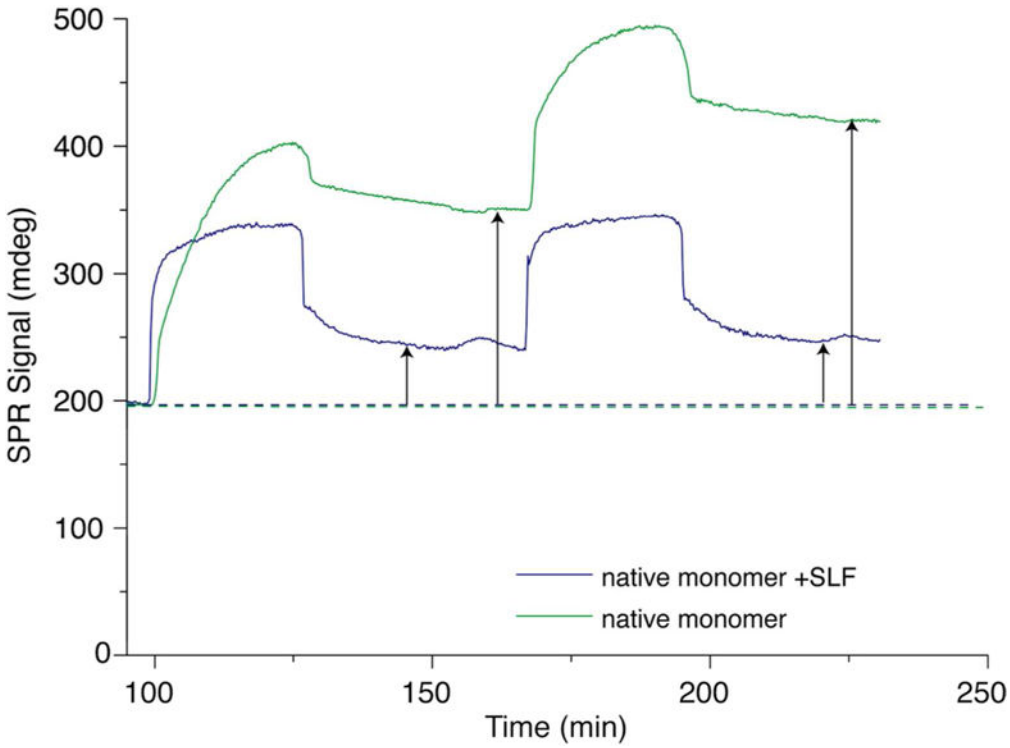

Fig. 8.

SLF inhibits Aβ self-association. MP-SPR signal response after injections of native monomeric Aβ (10 μM) over a surface of tethered Aβ monomers. Sample without SLF addition is shown by the green trace (lower channel). The same sample mixed with 20 μM SLF is given by the blue trace (upper channel). In both channels the mobile phase is the low ionic strength buffer, pH 8.0, with a flow rate of 10 μL/min.

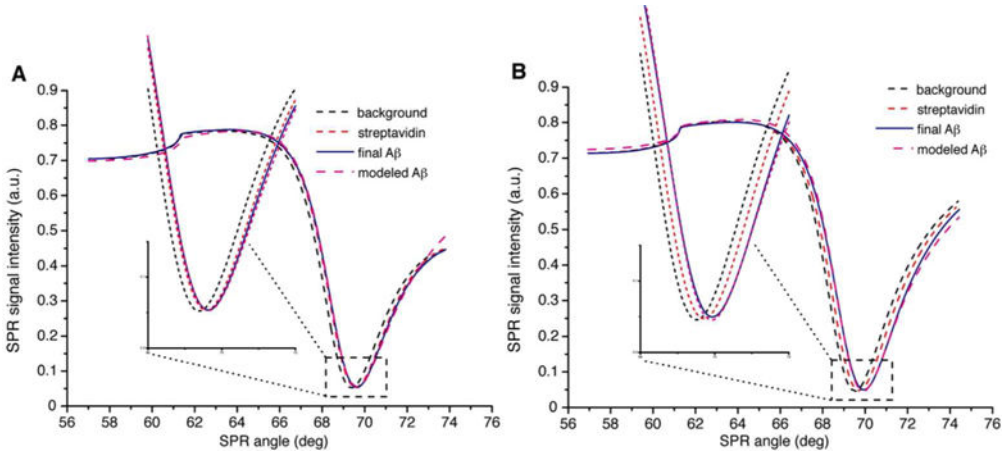

Fig. 9.

Layer modeling results for different situations of Aβ layer build-up. Panel **A** represents the biomolecular layer formation from the measurements in Fig. 8, where the SLF hampers the self-assembly processes of Aβ. Panel **B** shows the layer construction from the measurement in the absence of SLF, in Fig. 8, resulting in greater peptide aggregation (increased layer thickness). For clarity, the only the 670 nm laser data is shown.

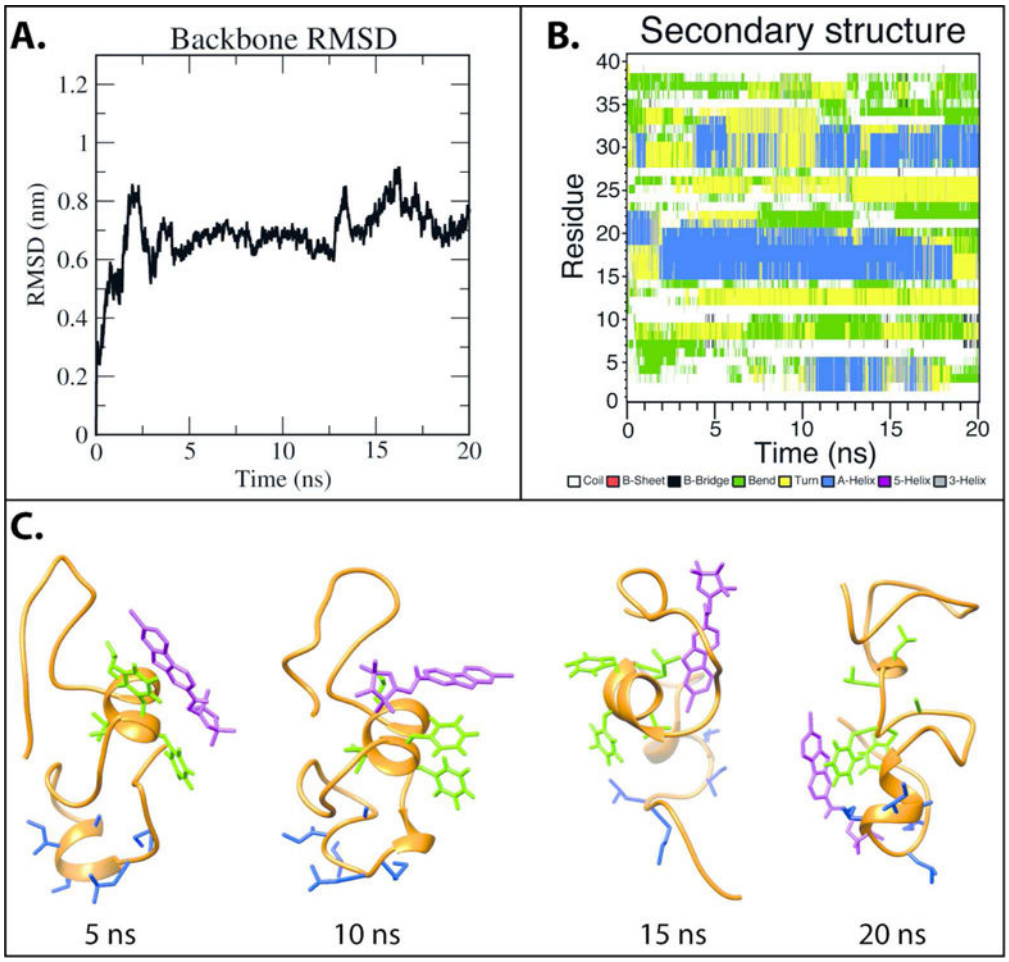

Fig. 10.

Docking calculation results for four snapshots derived from S1 simulation. (**A**) The secondary structure of the Aβ peptide as a function of S1 simulation time. Aβ has been rendered using cartoon representation and colored according to the secondary structure. (**B**) The root mean square deviation (RMSD) of the Aβ peptide backbone as a function of time. (**C**) The binding free-energies of SLF generated by the Autodock Vina are shown next to SLF molecules in kcal/mol (van der Waals representation). The backbone of the Aβ peptide is shown in orange. Residues 17-21 of Aβ (encompassing hydrophobic core I) are displayed in green. Residues 30-35 of Aβ (encompassing hydrophobic core II) are displayed in blue. The SLF molecule is displayed in magenta.

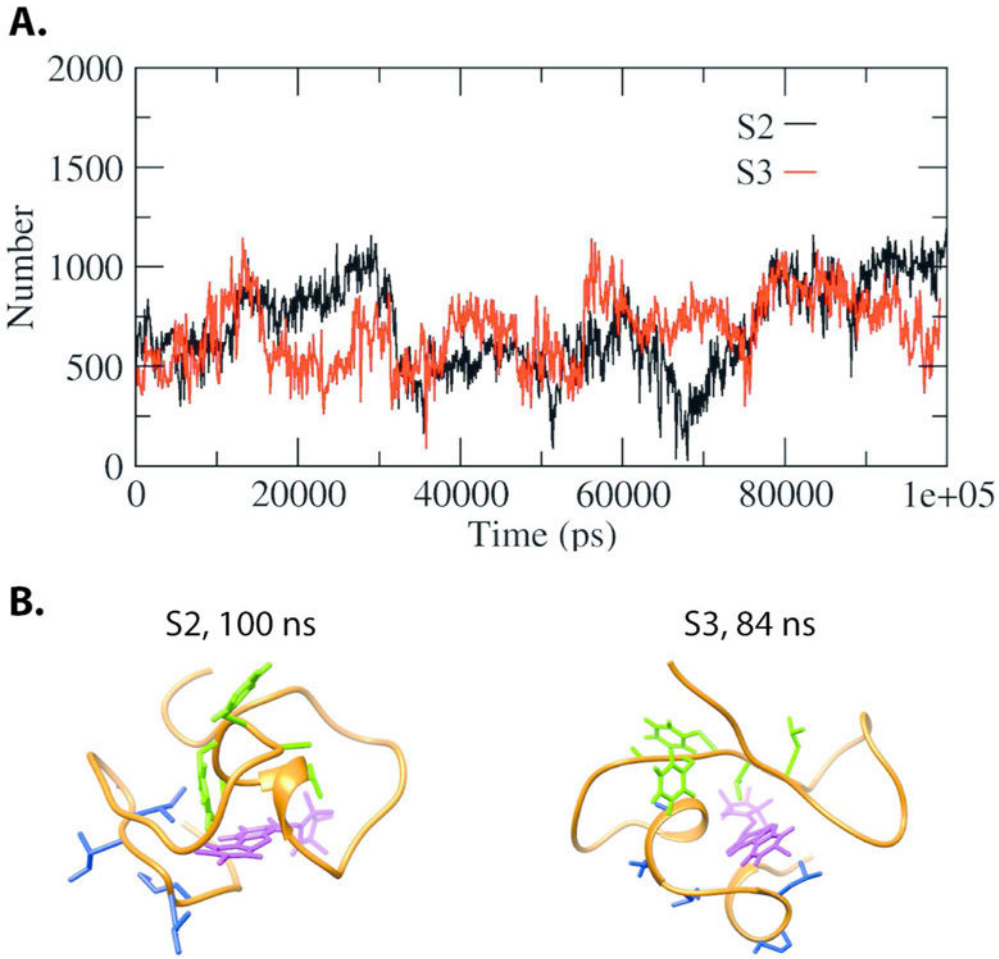

Fig. 11.

Stability of the S2 and S3 simulations. The number of contacts between SLF and the Aβ peptide as a function of simulation time are plotted in panel (**A**). Panel (**B**) shows snapshots of at the indicated time interval of simulation. The backbone of the Aβ peptide is shown in orange. Residues 17-21 of Aβ (encompassing hydrophobic core I) are displayed in green. Residues 30-35 of Aβ (encompassing hydrophobic core II) are displayed in blue. The SLF molecule is displayed in magenta.

Table 1

Affinity values determined for different interaction scenarios of Aβ/SLF binary complexes

Data was processed and fitted using TraceDrawer™ for MP-SPR Navi™. Values in parenthesis represent the statistical uncertainty.

	K_{D1} (M)	K_{D2} (M)	χ^2
SLF with biotinylated Aβ monomer	1.49×10^{-5} ($\pm 8.81\times10^{-7}$)	$<1\times10^{-9}$ *	34.39
SLF with native Aβ bound to biotinylated Aβ monomer	4.06×10^{-5} ($\pm 2.36\times10^{-6}$)	$<1\times10^{-9}$ *	23.30
SLF with AβO	1.08×10^{-4} ($\pm 1.48\times10^{-5}$)	1.21×10^{-4} ($\pm 1.80\times10^{-7}$)	41.63
SLF with AβO pretreated with SLF	1.15×10^{-4} ($\pm 1.06\times10^{-5}$)	9.84×10^{-5} ($\pm 1.11\times10^{-7}$)	44.63

* An upper limit for K_{D2} is given, as precision in fits cannot be obtained due to the limited dissociation of SLF binding in these samples.

Table 2

Layer thickness and refractive index calculations from the data in Fig. 9. For comparison, the hydrodynamic diameters of Aβ monomers and Aβ oligomers determined by DLS are shown.

Flow channel	Layer Thickness (nm)	Refractive Index
Upper (SLF present)	1.33	1.37139
Lower (SLF not present)	31.89	1.34070

Table 3

Simulated systems and the length of simulations.

	Simulation time	Molecules	Purpose
S1	5, 10, 15 and 20 ns	Aβ peptide + water	Generate discrete Aβ conformations for SLF docking and provide initial states for binary simulations (S2-S4)
S2	100 ns	1 Aβ peptide + 1 SLF + water	Simulate 1:1 SLF and Aβ interaction (from S1 @15 ns)
S3	100 ns	1 Aβ peptide + 1 SLF + water	Simulate 1:1 SLF and Aβ interaction (from S1 @20 ns)
S4	150ns	1 Aβ peptide + 2 SLFs + water	Simulate 2:1 SLF and Aβ interaction (from S1 @20 ns)